Mitochondrial Uncoupling Protein 2 Knockout Promotes Mitophagy to Prevent Retinal Ganglion Cell Death in Glaucoma

Abbreviated title: Ucp2 knockout protects RGCs from Glaucoma

Daniel T Hass and Colin J Barnstable, D.Phil.
Department of Neural and Behavioral Sciences, Penn State College of Medicine, 500 University Drive, Hershey, PA, USA 17033

Correspondence:
Colin J Barnstable, D. Phil.
Department of Neural and Behavioral Sciences
Penn State College of Medicine, Hershey, PA 17033, USA
cbarnstable@psu.edu

Abstract

Glaucoma is a neurodegenerative disorder characterized by mitochondrial dysfunction and an increase in oxidative damage leading to death of retinal ganglion cells (RGCs). The oxidative status of RGCs is regulated intrinsically, as well as extrinsically by retinal glia. The mitochondrial uncoupling protein 2 (UCP2) relieves oxidative and neuronal damage in a variety of neurodegenerative disease models. We hypothesized that deletion of *Ucp2* in either RGCs or retinal glia would increase retinal damage and retinal ganglion cell death in a mouse model of glaucoma. Paradoxically, we found the reverse, as deletion of mitochondrial UCP2 decreased oxidative protein modification and prevented retinal ganglion cell death in male and female mice. We resolved this paradox by finding that *Ucp2* deletion also increased levels of mitophagy in cell culture and markers of mitophagy in retinal tissue. Our data suggest that *Ucp2* deletion facilitates increased mitochondrial function by improving quality control. An increase in mitochondrial function explains the resistance of *Ucp2*-deleted retinas to glaucoma and may provide a therapeutic avenue for other chronic neurodegenerative conditions.

Significance Statement

Many unsolved neurodegenerative conditions result from defects in mitochondrial function. Molecular tools that can manipulate mitochondria will therefore be central to developing neuroprotective therapies. Among the most potent regulators of mitochondrial function are the uncoupling proteins, particularly UCP2. In this manuscript we show that while loss of UCP2 does increase mitochondrial membrane potential and the production of reactive oxygen species, it also initiates an increase in mitophagy that is ultimately neuroprotective. This novel protective consequence of uncoupling protein inhibition may lead to new therapeutic approaches to combat neurodegenerative disease, particularly because pharmacological compounds do exist that can selectively inhibit UCP2.

Introduction

Glaucoma is a group of disorders marked by progressive degeneration and death of retinal ganglion cells (RGCs) that leads to irreversible visual decline. Globally, glaucoma is the most frequent cause of irreversible blindness (Resnikoff and Keys, 2012). Primary open-angle glaucoma (POAG) is the most common form of the disease, and risk for POAG increases with age and elevated intra-ocular pressure (IOP) (Boland and Quigley, 2007; Tham et al., 2014). However, other signs such as a change in retinal morphology or loss of visual function are sufficient for a glaucoma diagnosis without an elevated IOP (Quigley, 2011).

Although glaucoma is often defined by the loss of RGCs, its pathophysiology is multifactorial and involves changes to multiple cell types within the inner retina, including müller glia and astrocytes (Varela and Hernandez, 1997; Carter-Dawson et al., 1998; Kawasaki et al., 2000; Woldemussie et al., 2004). During glaucoma, the mitochondria of these cell types become dysfunctional (Lee et al., 2011; Ju et al., 2015). Mitochondrial dysfunction can result in a bioenergetic deficit or increased levels of damaging reactive oxygen species (ROS) in the eye (Tanihara et al., 1997; Varela and Hernandez, 1997; Ferreira et al., 2010). The restoration of mitochondrial homeostasis and anti-oxidative support to both neurons and glia of the retina and optic nerve has become a major focus in research to prevent glaucomatous neurodegeneration (Kong et al., 2009; Lee et al., 2011; Garcia-Medina et al., 2014; Shen et al., 2015; Kimura et al., 2017).

Mitochondrial hydrogen peroxide production is highly dependent on mitochondrial pH and membrane potential (Ψ_m), and small decreases in Ψ_m or pH cause significant decreases in the production of reactive oxygen species (ROS) such as H_2O_2 (Korshunov et al., 1997; Miwa et al., 2003). The activity of exogenous agents that decrease Ψ_m cannot be easily regulated within cells and their use would risk a complete collapse of Ψ_m and thus ATP production. Alternatively, it is the prototypical function of endogenous uncoupling proteins to uncouple the electron transport chain from ATP synthase activity and decrease Ψ_m (Fleury et al., 1997; Echtay et al., 2001). The transcription, translation, and activity of endogenous uncoupling proteins are each regulated by multiple factors (Donadelli et al., 2014; Lapp et al., 2014).

There are 5 members of the uncoupling protein gene family (Bouillaud et al., 2001). The mitochondrial uncoupling protein 2 gene (*Ucp2*) is expressed in a variety of tissues, including the central nervous system (Pecqueur et al., 2001; Richard et al., 2001), and codes for a 309 amino acid protein (Fleury et al., 1997). UCP2 activity decreases electron transport chain efficiency, increasing energy expenditure (Zhang et al., 2001) and decreasing ROS generation (Nègre-Salvayre et al., 1997; Arsenijevic et al., 2000). UCP2-mediated uncoupling of mitochondria is cytoprotective under a variety of stressful conditions (Mattiasson et al., 2003; Andrews et al., 2005; Barnstable et al., 2016). As a consequence of *Ucp2* deletion, mice have more ROS and are more susceptible to cell death following acute exposure to stressors such as the dopamine cell toxin 1-methyl-4-phenyl-1,2,3,6-tetrahydropyridine (MPTP) (Andrews et al., 2005) or focal ischemia (Haines et al., 2010). Notably, Ucp2 deletion can be protective (de Bilbao et al., 2004), deleterious (Andrews et al., 2005; Haines et al., 2010), or have no clear effect on cell survival (Barnstable et al., 2016) in different models of neurodegeneration.

The goal of this study was to determine whether UCP2 normally functions to limit oxidative stress during glaucoma, thereby preventing a more severe form of the disorder. Glaucoma is a disease in which there are greater levels of ROS, and *Ucp2* deletion increases the generation of ROS (Arsenijevic et al., 2000). We therefore hypothesized that decreasing UCP2 levels would increase ROS and RGC death. However, our data suggest that by regulating mitochondrial dynamics, decreases in UCP2 levels can decrease the accumulation of oxidative damage to the retina and prevent retinal ganglion cell death.

Materials and Methods

Ethical approval

This study was carried out in accordance with the National Research Council's Guide for the Care and Use of Laboratory Animals (8th edition). The protocol was approved by the Pennsylvania State University College of Medicine Institutional Animal Care and Use Committee.

Animals

Wild-type (WT, C57BL/6J) and transgenic mice were housed in a room with an ambient temperature of 25°C, 30-70% humidity, a 12-hr light–dark cycle, and ad libitum access to rodent chow. Transgenic mouse strains, B6;129S-*Ucp2*$^{tm2.1Lowl}$/J (*Ucp2*$^{fl/fl}$, Stock#: 022394), B6.Cg-Tg(*GFAP-cre/ER*^{T2})505Fmv/J (*Gfap-creER*^{T2}, Stock#: 012849) (Ganat et al., 2006), and Tg(*Thy1-cre/ER*^{T2},-EYFP)HGfng/PyngJ (*Thy1-creER*^{T2}, Stock#: 012708) (Young et al., 2008) were each generated on a C57BL/6J background and purchased from the Jackson Laboratory (Bar Harbor, ME, USA). *Ucp2*$^{fl/fl}$ mice contain LoxP sites flanking exons 3 and 4 of the *Ucp2* gene. *Gfap-creER*^{T2} and *Thy1-creER*^{T2} mice express a fusion product of *cre* recombinase and an estrogen receptor regulatory subunit (*creER*^{T2}) under the control of the *hGFAP* or *Thy1* promoters. CreER^{T2} activity is regulated by the estrogen receptor modulator and tamoxifen metabolite 4-hydroxytamoxifen (Zhang et al., 1996), and in our studies, cre–mediated recombination of exons 3 and 4 of *Ucp2* was promoted in 1-2 month old mice by daily intra-peritoneal injections of 100 mg/kg tamoxifen (Sigma, T5648) dissolved in sunflower seed oil (Sigma, S5007) for 8 days. *Ucp2*$^{fl/fl}$ mice were injected with tamoxifen at the same time points as experimental subjects.

Breeding Scheme

To produce mice in which *Ucp2* is selectively deleted in *Gfap* or *Thy1*-expressing cells, *Ucp2*$^{fl/fl}$ mice were crossed with *Gfap-creER*^{T2} or *Thy1-creER*^{T2} mice, and *Ucp2*$^{fl/+}$; *creER*^{T2}-positive offspring were crossed with *Ucp2*$^{fl/fl}$ mice. The resulting *Ucp2*$^{fl/fl}$*; Gfap-creER*^{T2} or *Ucp2*$^{fl/fl}$*; Thy1-creER*^{T2} offspring were bred with *Ucp2*$^{fl/fl}$, and the offspring of these pairings were used in this study.

IOP Measurement

Intra-ocular pressure (IOP) was measured in isoflurane-anesthetized mice using an Icare® TonoLab (Icare Finland Oy, Espoo, Finland) rebound tonometer, both before and after injection with polystyrene microbeads. Each reported measurement per mouse per eye is the average of 18 technical replicates. Though the amount of time

under anesthesia has been shown to affect IOP (Ding et al., 2011), mice were anesthetized for <10 minutes and yielded stable mean IOP measurements, particularly in control eyes. However, the work of Ding et al., 2011 leads us to believe that our method of measurement underestimates IOP values by at least 3 mmHg, and possibly more in bead-injected eyes (Ding et al., 2011). Mice were only included in this study if their IOP was elevated by 3 mmHg, or if a t-test of their IOP over time between bead and PBS-injected eyes was statistically significant.

Genotyping

Tissue from ear punches was lysed and digested for genotyping. *Ucp2*$^{fl/fl}$ mice were genotyped with PCR primers flanking a LoxP site on the *Ucp2* gene (Table 1, *Ucp2*^{flox}). To determine whether CreER^{T2}-mediated *Ucp2* exon3-4 excision had occurred within a subset of samples, the reverse primer was used together with a primer outside the LoxP-flanked region (Table 1, *Ucp2*$^{\Delta}$). PCR conditions to amplify *Ucp2*^{Flox} or *Ucp2*$^{\Delta}$ were as follows: (**1**) 95°C–3 min, (**2**) 95°C–1 min, (**3**) 73°C–1 min, (**4**) 72°C–30 seconds, (**5**) Go to (2) for 15 cycles (-1°C/cycle), (**6**) 95°C–1 min, (**7**) 58°C–1 min, (**8**) 72°C–30 seconds, (**9**) Go to (6) for 20 cycles, (**10**) 95°C–10 min, (**11**) Hold at 4°C. Both the *Thy1-CreER*^{T2} and *Gfap-CreER*^{T2} genes were genotyped using primers binding to an internal region of *Cre* recombinase (Table 1, Cre). PCR conditions to amplify *Cre* were as follows: (**1**) 95°C–3 min, (**2**) 95°C–1 min, (**3**) 58.1°C–1 min, (**4**) 72°C–30 seconds, (**5**) Go to (2) for 29 cycles, 95°C–10 min, **(6**) Hold at 4°C (Ganat et al., 2006).

Microbead Injection

We modeled glaucoma in mice by elevating IOP. We increased IOP in 2-4 month old *Ucp2*$^{fl/fl}$, *Ucp2*$^{fl/fl}$*; Gfap-creER*^{T2}, and *Ucp2*$^{fl/fl}$; *Thy1-creER*^{T2} mice of both genders similarly to the Cone et al. '4+1' protocol (Sappington et al., 2010; Cone et al., 2012). At least 24 hours prior to bead injection, we took a baseline IOP measurement to confirm that a given mouse had a 'normotensive' IOP. We found that prior to bead injection, IOP is very stable and can be well represented by a single pre-bead measurement (data not shown). We then anesthetized mice with an intraperitoneal (IP) injection of 100 mg/kg Ketamine and 10 mg/kg Xylazine, and treated each eye with topical proparacaine hydrochloride (0.5%) to further anesthetize and hydrate the cornea during injections. We then sterilized 1- and 6-µm diameter polystyrene microbeads (Polysciences, Cat#: 07310-15 and 07312-5) as noted in Cone et al., and estimated bead concentrations on a hemocytometer. We injected 2 µL of 6 µm (at $3x10^6$ beads/µL) and 2 µL of 1 µm (at $1.5x10^7$ beads/µL) microbeads through the cornea using a 50-100 µm cannula formed by a beveled glass micropipette connected by polyethylene tubing to a Hamilton syringe (Hamilton Company Reno, NV, USA). As an internal control, the same volume of sterile 1x phosphate buffered saline (PBS) was injected into the contralateral eye. We measured postoperative IOP every 3 days for 3 to measure changes in gene expression, mtDNA/nDNA, or mitochondrial function, or 30 days for all other forms of analysis. Following the terminal IOP measurement, mice were asphyxiated using a Euthanex SmartBox system, which automatically controls CO_2 dispersion, followed by cervical dislocation. Figure 1B illustrates a visual representation of this experimental design.

Cytochrome-C oxidase Histochemistry

Cytochrome-C oxidase (COX) activity was assayed using a modified procedure described by (Wong-Riley, 1979; Murphy et al., 2012). Briefly, following euthanasia, unfixed mouse eyes were harvested, immediately frozen in OCT on dry ice, and cut in to 10 µm sections. Control and experimental samples were frozen and sectioned on the same slide to minimize potential slide-to-slide variability. Slides were incubated in an assay solution containing 4 mM 3',3'-diamidobenzadine, 100 µM cytochrome C (Sigma, Cat#: 2037), and 5 U/mL catalase (Sigma, Cat#: E3289) for 1h at 37°C. Assay control slides were additionally exposed to 5 mM NaN_3, which inhibits COX activity.

Histology and Immunocytochemistry

Immunolabeling of sectioned retinal tissue was performed as previously described (Pinzon-Guzman et al., 2011). Briefly, whole eyes were fixed in 4% paraformaldehyde (Electron Microscopy Sciences, Hatfield, PA, USA) in 1x PBS overnight at 4°C. The next day, eyes were divided in half with a scalpel blade. One half was frozen and sectioned, while the other was labeled as a whole-mount. Frozen tissue were embedded in a 2:1 mixture of 20% sucrose and OCT (Electron Microscopy Sciences), cooled to -20°C, and cut at a 10 µm thickness. Samples for each experiment were located on the same slide to control for assay variability. Prior to immunohistochemical labeling, we unmasked antigens in a pH 6.0 sodium citrate buffer. Sections were permeabilized with 0.2% Triton-X-100 in PBS, blocked with 5% nonfat milk, and incubated in primary antibodies (Table 2) overnight at 4 °C. The following day, sections were washed and incubated in secondary antibody for 3 hours, followed by incubation in 1 µg/mL Hochest-33258 for 20 minutes. After three washes, slides were mounted with 0.5% n-propyl gallate in 1:1 glycerol: PBS. Retinal whole mounts used a similar protocol but with the following modifications: antigens were not unmasked, tissue was incubated in primary antibody for 6 days at 4°C and secondary overnight at 4°C. Labeled tissue was imaged on an Fluoview FV1000 confocal microscope (Olympus). In each experiment, acquisition parameters for a given antibody were held constant. RGCs were counted using the marker RBPMS (Rodriguez et al., 2014) in tissue whole-mounts 1000 µM from the optic nerve head, and the counter was blinded to the identity of each sample. All fluorescent labeling intensity measurements were derived using the ImageJ measurement tool. We measured colocalization between LC3B and TOMM20 using the ImageJ plugin "Coloc 2" and reporting the Manders' overlap coefficient corresponding to the TOMM20 image channel. Unless otherwise specified, intensity measurements were bounded by the ganglion cell layer and the outer nuclear layer.

RNA Isolation and Quantitative Real-Time PCR

Frozen tissue was lysed in TRIzol (Thermo-Fischer, Cat#:15596018) and RNA precipitated using the manufacturer's recommended procedure. Final RNA concentration was measured using a NanoDrop ND-1000 Spectrophotometer prior to reverse transcription. We reverse transcribed RNA using SuperScript III (Thermo-Fischer, Cat#: 18080093) with random hexamers. Genomic and mitochondrial DNA amplified via qPCR was isolated using a DNeasy Blood and Tissue kit (Qiagen, Cat#: 69504) in accordance with the manufactures' specifications. DNA was amplified with iQ

SYBR Green Supermix (Bio-Rad, Cat#: 1708882) and quantitated on a Bio-Rad iCycler. All primers designed to measure gene expression (Table 1) do not amplify genomic sequences, and qPCR reactions were followed by a melt curve analysis to confirm the amplification of a single PCR product. All results were normalized against the TATA-box binding protein (*Tbp*) cDNA using the $\Delta\Delta C_t$ method. *Tbp* is stably expressed during both mouse retinal development (Adachi et al., 2015) and in retinal endothelial cells treated with innate immune system stimulants (Wei et al., 2013).

Primary Astrocyte Culture

Primary mouse cortical astrocytes were isolated from postnatal day 1-4 mice as previously described (Sarafian et al., 2010; Lapp et al., 2014). Briefly, mice were decapitated and brains were removed from the skull. In tissue culture medium, a ~1 cm portion of superior cerebral cortex was pinched off of the brain using curved forceps. Meninges were removed, and the tissue was triturated with a sterile flame-polished glass Pasteur pipette until it formed a single cell suspension, approximately 20x. The suspension was filtered through a 70 µm cell strainer to remove larger debris, centrifuged at 500 x g and 4°C for 5 min, resuspended in growth medium (Dulbecco's Modified Eagle's Medium/Ham's F12 supplemented with 2 mM L-glutamine, 15 mM HEPES, 10% fetal bovine serum, and 10 ng/mL gentamicin), and plated in a T-25 tissue culture flask. Cells were grown at 37°C in a 5% CO_2/balance air atmosphere. After the cells have reached confluence between 7-14 days in vitro (DIV), contaminating cells were shaken off at 250 RPM overnight and growth medium was replaced. Astrocyte-enriched cultures were then passaged at least 48 hours following medium replacement for experimentation, and used for experimentation at passage #2 or 3. All cells used in this study were exposed to 1 µM 4-hydroxytamoxifen (Sigma, Cat#: H6278) for 24 hours prior to studies of *Ucp2* function.

Measurement of Mitochondrial Membrane Potential and Oxidative Status

We determined mitochondrial membrane potential (Ψ_m) and relative oxidative status were determined on a fluorescence-enabled microplate reader (BioTek Synergy II) using black tissue-culture-treated 96-well plates (Corning, Cat#3603) seeded with 30,000 cells/well. We treated all primary astrocytes from *Ucp2*$^{fl/fl}$ and *Ucp2*$^{fl/fl}$*; Gfap-creER*^{T2} mice with 4-hydroxytamoxifen and washed it out at least 24 hours prior to the assay. To measure membrane potential, we loaded cells with 5,5',6,6'-tetrachloro-1,1',3,3'-tetraethyl-benzimidazolylcarbocyanine iodide (JC-1; 2 µg/mL; Thermo-Fischer, Cat#: T3168) in culture medium for 30 min. We measured red and green fluorescence 5 minutes after washing out each probe. Each assay contained controls treated with the membrane permeant protonophore Carbonyl cyanide-*4*-(trifluoromethoxy) phenyl-hydrazone (FCCP, 1 µM, Caymen Chemical). We determined the effect of UCP2 on oxidant production using the redox-sensitive probe Chloromethyl–2′,7′-di-chlorofluorescein diacetate (CM-H_2-DCFDA, 40 µM; Thermo-Fischer, Cat#: C6827) in 1x PBS supplemented with 1 mM glucose and 2 mM GlutaMax (Thermo-Fischer, Cat#: 35050-061). The probe was washed out following a 30-minute incubation. We measured oxidant production in the plate reader's kinetic mode, which took serial measurements of CM-H_2-DCFDA fluorescence over time. The increase in fluorescence (ΔF) over 30 minutes was divided by initial fluorescent intensity (F_0). This rate of

increase in CM-H_2-DCFDA fluorescence was normalized to the mean $\Delta F/F_0$ of *Ucp2*$^{fl/fl}$ cells to minimize inter-assay variability.

Extracellular Flux Analysis

Oxygen consumption (OCR) and extracellular acidification rate (ECAR) were used as proxies of oxidative and glycolytic metabolism, respectively. We performed a 'mitochondrial stress test' on cultured astrocytes (seeded at 30,000 cells/well) using inhibitors of electron transport at the indicated final concentrations: oligomycin (25 µg/mL; Caymen Chemical), FCCP (1 µM), antimycin A (1 µM), and rotenone (1 µM). Following the assay, we measured DNA concentration in each well for normalization of OCR traces.

Statistical analysis

We performed all statistical analyses in GraphPad Prism. We determined the statistical effect of one independent variable on 2 groups used a Student's t-test or paired sample t-test in cases where samples were matched (e.g. the control was the contralateral eye of the same animal). We analyzed the effect of one variable on >2 groups using a one-way ANOVA with a Bonferroni's post-hoc analysis. We analyzed the effect of 2 variables using a 2-way ANOVA with a Bonferroni's post-hoc analysis. The statistical significance threshold was $p<0.05$ for all tests.

Results

UCP2 Localization in the Retina and Characteristics of the Microbead Model

To confirm that UCP2 is normally present in the retina and to determine its cellular localization, we immunolabeled fixed retinal tissue from wild-type C57BL6/J and whole-body *Ucp2* knockout mice (courtesy of Dr. Tamas Horvath). Retinas from *Ucp2*-knockout mice were used as a control for antibody specificity. UCP2 was distributed throughout the mouse retina, with strong expression within the retinal ganglion cell layer (GCL) and photoreceptor inner segments (upper panel, Fig. 1A). In order to study the actions of UCP2 in a mouse model of glaucoma, we implemented a microbead model that elevates intra-ocular pressure (IOP), illustrated in Figure 1B. Prior to further studies, we confirmed that neither gender nor genotype had an effect on the baseline IOP characteristics of the mouse eye (Fig. 1C). We also confirmed that injection of microbeads in to the anterior chamber of the eye resulted in their migration to the aqueous humor outflow pathway, at the irido-corneal angle (Fig. 1D). Finally, we found a relationship between the bead-induced increase in IOP and a decrease in RGC survival, measured by a decrease in the density of RBPMS+ retinal ganglion cells in retinal whole-mounts (Fig. 1E).

Elevated IOP decreases mitochondrial function and increases oxidative stress

One stable mark of oxidative damage is accumulation of lipid peroxidation products such as 4-hydroxy-2-nonenal (HNE). HNE can modify histidine residues on proteins, forming a stable adduct that we used as a proxy for oxidative stress in tissue. To determine whether the retina is oxidatively stressed in the microbead glaucoma model, we compared HNE labeling in the retinal layers of microbead- and PBS-injected eyes. Microbead-injection significantly increased HNE reactivity in the inner retina to

159±29% of contralateral PBS-injected eyes (p=0.0035, df=36, n=5), but not in the outer retina (98±23% of contralateral control). Analysis of individual inner retinal layers showed increases in HNE but none of these reach significance following adjustment for multiple comparisons, suggesting that the effects of IOP on oxidative stress occur in multiple cell types (Fig 2A-B). To determine the effect of IOP elevation on mitochondrial function, we tested cytochrome oxidase (COX) activity in fresh-frozen slices of retina from PBS- and Bead-injected mice and found that by 3 days post bead-injection, there was a significant decrease in retinal cytochrome oxidase activity (p=0.0313, df=4, n=5, Fig. 2C). The decrease in COX activity preceded a decrease in mitochondrial copy number, determined by the mtDNA/nDNA ratio (Lee et al., 2014). Relative to contralateral eyes, mtDNA/nDNA was not altered 3 days following bead injection (t-test, ns, n=3), but was significantly decreased (52±8%) by 30 days (p=0.041, df=9, n=8, Fig. 1D). We also determined the expression of the oxidative stress and glaucoma related genes *Hmox1*, *Nfe2l2*, *C1Qa*, *Ucp2*, *Sod2*, and *C1Qa* in untreated (naïve) retinas, PBS-injected, and microbead-injected retinas, 3 days post bead injection (n=3, df=6). Bead-injection increased the expression of *Hmox1* (856±294%, p=0.019), *Nfe2l2* (149±14%, p=0.029), and *C1Qa* (728±295%, p=0.043) relative to contralateral bead-injected retinas, and caused smaller, non-significant increases in *Sod2* (117±35%, ns) and notably in *Ucp2* as well (366±196%, ns, Fig. 2E). In all cases, the expression of these genes was unchanged between naïve and PBS-injected retinas. In all subsequent experiments we used contralateral PBS-injected retinas as a control for microbead-induced IOP elevation.

Ucp2 Deletion Increases Mitochondrial Membrane Potential (Ψ_m) and Oxidative Stress

To investigate the effects of *Ucp2* deletion on cellular function, we used primary cortical astrocytes cells from *Ucp2*$^{fl/fl}$ and *Ucp2*$^{fl/fl}$*; Gfap-creER*^{T2} mice. In figure 3A (II) we show a schematic diagram of the floxed *Ucp2*, including the region excised by cre recombinase, and the PCR primers used to diagnose genotype or cre recombination. We also show the two different variants of cre used in this study (I) as well as (III) a schematic indicating which figures use primary cells and which used retinal tissue. In figure 3B we show an example gel from 4-hydroxytamoxifen-pretreated *Ucp2*$^{fl/fl}$ (Fig. 3B, lanes 1-2) and *Ucp2*$^{fl/fl}$*; Gfap-creER*^{T2} astrocytes (lanes 3-4), from which we amplified a PCR product (Ucp2$^{\Delta}$) that is only detected in cre-expressing cells, following cre-mediated *Ucp2* exon3-4 excision. We determined the effect of *Ucp2* on mitochondrial transmembrane potential (Ψ_m), oxidative stress, and cell respiration using these astrocytes. We measured Ψ_m using the vital dye JC-1, which equilibrates in mitochondria as red fluorescent aggregates and outside as green fluorescent monomers. The ratio of aggregate/monomers is proportional to Ψ_m, and we found that *Ucp2* deletion increased Ψ_m to 120±7% of control samples (p=0.026, df=15, n=7-8). As a control, we applied the membrane-permeant protonophore FCCP (1 μM), which reduced Ψ_m to 72±4% of controls (p=0.013, df=15, Fig. 3C). Oxidative stress was measured using CM-H_2-DCFDA, a cell permeant probe that becomes fluorescent upon oxidation, and we measured the rate ($\Delta F/F_0$) of probe oxidation over 30 minutes. Relative to *Ucp2*$^{fl/fl}$ controls, *Ucp2* deletion increased oxidative stress to 133±12% (p=0.0452, df=16, n=7). As a control to verify assay function, *Ucp2*$^{fl/fl}$ cells were treated with 4 μM Antimycin A, which also increased oxidative stress to 122±10% of controls

(ns, df=16, n=5, Fig 3D). We measured oxygen consumption rate using a seahorse extracellular flux assay in *Ucp2*$^{fl/fl}$ and *Ucp2*$^{fl/fl}$*; Gfap-creER*^{T2} astrocytes. Following each assay we normalized respiratory activity to DNA concentration. Basal respiration (untreated) over time was greater in *Ucp2*$^{fl/fl}$*; Gfap-creER*^{T2} cells (p<0.0001, df=1, n=3), as was maximal respiration (p=0.0004, df=1, n=3), suggesting greater mitochondrial function in cells lacking a functional copy of *Ucp2* (Fig. 3E).

Ucp2 deletion prevents retinal ganglion cell loss during glaucoma

Cre-mediated *Ucp2* deletion was confirmed by measuring transcript levels, which were decreased in the retinas of tamoxifen-pretreated *Ucp2*$^{fl/fl}$*; Gfap-creER*^{T2} and *Ucp2*$^{fl/fl}$; *Thy1-creER*^{T2} mice to 62±16% and 68±17% of *Ucp2*$^{fl/fl}$, respectively (Fig. 4A). Mice with *Ucp2* selectively deleted in *Gfap* or *Thy1*-expressing cells were subjected to intraocular bead injection. Using reporter mice in which EGFP or YFP are co-expressed with *cre* recombinase, we confirmed the localization of these *cre* variants to retinal glia or ganglion cells (Fig. 4B). We injected beads in to mice with *Ucp2* selectively deleted in *Gfap* or *Thy1*-expressing cells. On average, bead injection increased mean IOP from 9.7±0.2 to 18.7±1.8 mmHg in *Ucp2*$^{fl/fl}$ mice, from 10.9±0.5 to 14.1±1.2 mmHg in *Ucp2*$^{fl/fl}$*; Gfap-creER*^{T2} mice, and from 10.4±0.4 to 20.6±2.2 mmHg in *Ucp2*$^{fl/fl}$; *Thy1-creER*^{T2} mice (Fig. 4C). Figure 1E shows that either a 4-5 mmHg or a >10 mmHg increase in IOP is sufficient to induce the same extent of RGC loss, so differences in the extent of IOP increase between *Ucp2*$^{fl/fl}$*, Ucp2*$^{fl/fl}$; *Thy1-creER*^{T2}, and *Ucp2*$^{fl/fl}$; *Gfap-creER*^{T2} mice should not alter retinal ganglion cell death. To determine the effect of *Ucp2* deficiency on glaucomatous RGC death, we counted the density of RBPMS+ RGCs on whole-mount retinas from *Ucp2*$^{fl/fl}$, *Ucp2*$^{fl/fl}$*; Gfap-creER*^{T2} and *Ucp2*$^{fl/fl}$; *Thy1-creER*^{T2} retinas (Fig. 4D). We determined the effect of glaucoma on RGC density using a 2-way ANOVA with Genotype and Bead-Injection as independent variables. A Bonferroni post-hoc analysis revealed that bead-injection significantly decreased retinal RGC density by 607±148 cells/mm^2 in *Ucp2*$^{fl/fl}$ retinas (df=49, n=29), but not in *Ucp2*$^{fl/fl}$*; Gfap-creER*^{T2} (-201±196 cells/mm^2, p=0.0063, n=10) or *Ucp2*$^{fl/fl}$; *Thy1-creER*^{T2} retinas cells/mm^2, (-169±151 cells/mm^2, p=0.0039, n=13, Fig. 4D-E). These data suggest that surprisingly, lack of UCP2 in the retina decreases the damage to RGCs caused by IOP elevation.

The Mechanism of Ucp2-deletion mediated neuroprotection

To determine the effect of UCP2 on retinal oxidative stress, we measured HNE immunoreactivity in the retinas of bead-injected eyes from *Ucp2*$^{fl/fl}$, *Ucp2*$^{fl/fl}$*; Gfap-creER*^{T2} and *Ucp2*$^{fl/fl}$; *Thy1-creER*^{T2} mice (Fig. 5A-B). Relative to *Ucp2*$^{fl/fl}$ controls, both bead-injected *Ucp2*$^{fl/fl}$; *Thy1-creER*^{T2} (65.1±7.4% of control) and *Ucp2*$^{fl/fl}$*; Gfap-creER*^{T2} (69.8±7.8% of control) accumulated significantly less HNE (p=0.030 and 0.011 respectively, df=20, n=7-8), suggesting that the inner retina was less oxidatively stressed (Fig. 5B). Increases in GFAP are a sign of glial cell activation, and in *Ucp2*$^{fl/fl}$ mice, bead injection increased GFAP intensity to 239% of control (p=0.0085, df=61, n=13-23). In *Ucp2*$^{fl/fl}$*; Gfap-creER*^{T2} or *Ucp2*$^{fl/fl}$; *Thy1-creER*^{T2}, bead injection did not significantly increase GFAP labeling intensity, though there was a trend toward increase for each genotype (Fig. 5C). In addition to the UCP2-deletion specific decreases in HNE and GFAP labeling, there was an increase in mtDNA/nDNA in *Ucp2*$^{fl/fl}$; *Thy1-creER*^{T2} retinas relative to *Ucp2*$^{fl/fl}$ controls (12629±2271 to 29475±7441, p=0.040, df=13, n=4-

8). A similar difference was not seen between *Ucp2*$^{fl/fl}$ and *Ucp2*$^{fl/fl}$*; Gfap-creER*^{T2} sections (Fig. 5D). We hypothesized that because mitochondria are less dense in retinal glia than in ganglion cells, a change in glial mtDNA/nDNA may occur and not be detectable in the retina. To test whether *Ucp2* deletion alters mitochondrial copy number in glia, we used primary cultures of cortical astrocytes, and found that *Ucp2* deletion did increase mtDNA/nDNA levels (p= 0.023, df=4, n= 3, Fig. 6A).

We next determined the expression of three genes involved in mitochondrial biogenesis, *PolgA, Tfam,* and *PGC1-α.* These genes were not significantly altered by *Ucp2* deletion in primary *Ucp2*$^{fl/fl}$*; Gfap-creER*^{T2} astrocytes, though the expression of nuclear and mitochondrial genes associated with mitochondrial function (*CytB*, *Sod2)* were significantly decreased (p=0.037 and 0.024 respectively, df=27, n=3-4, Fig. 6B). Since the UCP2-dependent alteration in mtDNA/nDNA did not appear to be due to a change in mitochondrial biogenesis, it may have resulted from an increase in degradation through mitochondrial autophagy ("mitophagy"). To test this, we measured the subcellular distributions of the autophagosome protein LC3B and the mitochondrial marker Tomm20 in primary cultures of cortical astrocytes (Fig. 6C-D). Using the Coloc2 plugin on ImageJ, we determined the Manders' overlap coefficient corresponding to the proportion of co-localized (LC3B+ Tomm20+) pixels over Tomm20+ pixels (tM2). *Ucp2* deletion significantly increased tM2 from 0.044±0.019 to 0.128±0.024 (p=0.033, df=6, n=3-4, Fig. 6D). tM2 also increased to a greater extent in *Ucp2*$^{fl/fl}$ astrocytes treated with 10 μM FCCP for 3h, a treatment known to reproducibly induce mitochondrial fragmentation and mitophagy (0.246±0.074). Mitochondria destined for destruction become porous, so if mtDNA escapes from these damaged mitochondria to the cytosol and avoided destruction, it would explain elevated mtDNA/nDNA levels in *Ucp2*$^{fl/fl}$*; Gfap-creER*^{T2} astrocytes and in *Ucp2*$^{fl/fl}$; *Thy1-creER*^{T2} retinas. However we fount this unlikely, as the cytosolic DNA sensing pathway intermediate IRF3 was not localized to the nucleus of *Ucp2*$^{fl/fl}$*; Gfap-creER*^{T2} cells (Fig. 6E).

We performed similar forms of analysis on retinal tissue to determine whether *Ucp2* impacts mitochondrial biogenesis or markers of mitophagy. Similar to our findings in astrocytes, we found no difference in the expression of *PolgA, Tfam,* and *PGC1-α* (Fig. 7A). Although mitochondria are too dense in retinal tissue to perform an accurate colocalization analysis for Tomm20 and LC3, we determined the extent of retinal autophagy by measuring LC3B labeling in bead-injected *Ucp2*$^{fl/fl}$*, Ucp2*$^{fl/fl}$*; Gfap-creER*^{T2}*,* and *Ucp2*$^{fl/fl}$; *Thy1-creER*^{T2} retinas. Relative to *Ucp2*$^{fl/fl}$ retinas (n=5), there was a significant increase in retinal LC3B intensity in bead-injected *Ucp2*$^{fl/fl}$; *Thy1-creER*^{T2} (317.2±43.3% of control, ANOVA, p=0.006, df=8, n=3) and *Ucp2*$^{fl/fl}$*; Gfap-creER*^{T2} retinas (581.9±36.1% of control, p=0.0001, df=8, n=3) (Fig. 5E-F), suggesting that *Ucp2* deletion results in greater levels of autophagy within both cell types of the retina (Fig. 7B-C).

Discussion

Mitochondrial dysfunction and oxidative stress are central to the pathophysiology of glaucoma and have been observed in both animal models and human tissue (Moreno et al., 2004; Malone and Hernandez, 2007; Lee et al., 2011; Mousa et al., 2015; Khawaja et al., 2016). Following a microbead injection, we confirmed the role of

elevated IOP in RGC death (Fig. 1), mitochondrial dysfunction, and oxidative stress (Fig. 2).

Previous studies have shown that greater levels of *Ucp2* expression is protective against various conditions that increase oxidative stress, including excitotoxicity and MPTP-induced parkinsonism (Diano et al., 2003; Andrews et al., 2005; Barnstable et al., 2016). We have found that UCP2 is highly expressed in the inner retina (Fig. 1A), an area greatly affected by oxidative stress in glaucoma, and have verified its role in the regulation of Ψ_m and oxidative stress in a cellular system (Fig. 3C-D). Muller glia, astrocytes, and RGCs all exist within the inner retina and each regulate the bioenergetic and oxidative status of ganglion cells (Kawasaki et al., 2000).

To determine whether UCP2 alters the progression of glaucoma, and the cell types within which its actions are most important, we used mice in which *Ucp2* was selectively deleted in *Gfap*-expressing (astrocytes and müller glia) or in *Thy1*-expressing cells (retinal ganglion cells; Fig. 4). We increased the IOP of these mice by injecting microbeads and found that while an elevated IOP may increase RGC loss (Fig. 4C-E), reactive gliosis (Fig. 5C) and retinal damage (Fig. 5A-B) in *Ucp2*$^{fl/fl}$ control mice, *Ucp2*$^{fl/fl}$*; Gfap-creER*^{T2} and *Ucp2*$^{fl/fl}$*; Thy1-creER*^{T2} were both protected from these phenotypes. This finding, while not unprecedented (de Bilbao et al., 2004), was surprising, as *Ucp2* overexpression is neuroprotective in retinas exposed to excitotoxic factors (Barnstable et al., 2016). We found that the decrease in gliosis, oxidative damage, and RGC loss corresponded to a curious increase in the mtDNA/nDNA of *Ucp2*$^{fl/fl}$; *Thy1-creER*^{T2} retinas but not in *Ucp2*$^{fl/fl}$*; Gfap-creER*^{T2} retinas (Fig 5D). We believe that analysis of retinal mtDNA/nDNA is more sensitive to RGCs as they have a high density of mitochondria, and when we investigated the mtDNA/nDNA in primary astrocytes, we also found a significant increase following *Ucp2* deletion (Fig. 6A). These findings led us to investigate the role that *Ucp2* might play in regulating mitochondrial dynamics.

We first investigated mitochondrial biogenesis, which did not appear to be correlated with mtDNA/nDNA, as *Tfam*, *Pgc1-α*, and *PolgA* were unchanged by *Ucp2* deletion in culture or in *Ucp2*$^{fl/fl}$; *Thy1-creER*^{T2} and *Ucp2*$^{fl/fl}$*; Gfap-creER*^{T2} retinas (Fig. 6B and 7A). However, the expression of the mitochondrial genes *CytB* and *Sod2* was significantly decreased in *Ucp2*$^{fl/fl}$*; Gfap-creER*^{T2} astrocytes, leading us to investigate the effect of *Ucp2* deletion on the degradation of mitochondria, dubbed mitophagy. Mitophagy is a form a quality control in which damaged mitochondria are selectively degraded (Kim et al., 2007). We found greater levels of mitophagy in *Ucp2* deleted astrocytes (Fig. 6C-D), and confirmed that the marker of autophagy, LC3B, was significantly increased in the retinas of *Ucp2*$^{fl/fl}$; *Gfap-creER*^{T2} and *Thy1-creER*^{T2} mice (Fig. 7B-C). The increase in LC3B was greatest in *Ucp2*$^{fl/fl}$*; Gfap-creER*^{T2} retinas, suggesting that loss of *Ucp2* in astrocyte and müller glia strongly activates mitophagy. Retinal glia are phagocytic cells (Bejarano-Escobar et al., 2017), and astrocytes of the optic nerve head are specifically able to phagocytose and dispose of damaged RGC mitochondria (Davis et al., 2014). If a Ucp2-deletion dependent increase in glial mitophagy increases the disposal of RGC mitochondria, it would explain why *Ucp2*$^{fl/fl}$*; Gfap-creER*^{T2} mice are protected from glaucoma. *Ucp2*$^{fl/fl}$*; Thy1-creER*^{T2} mice are most likely protected from glaucoma because *Ucp2* deletion within RGCs is expected to directly increase mitophagy.

Our data suggest that *Ucp2* deletion increases mitochondrial quality control, clearing damaged mitochondria and improving bulk mitochondrial function. These data are supported by a previous study, which found that *Ucp2* deletion increases mitophagy in pulmonary endothelial cells (Haslip et al., 2015). An effect of UCP2 on mitophagy would also explain how *Ucp2* deletion increases basal and maximal (FCCP-induced) astrocyte respiration without altering oligomycin-insensitive respiration (Fig. 3E), as having a greater proportion of functional mitochondria can increase a cell's capacity for respiration (Drew et al., 2014). While these data are contrary to the canonical function of an uncoupling protein, the process of mitophagy specifically selects dysfunctional mitochondria for degradation (Lemasters, 2005; Kim and Lemasters, 2011) and this activity could result in cells enriched for undamaged mitochondria. Greater levels of mitophagy can protect the retina from glaucoma, as a study recently demonstrated by manipulating levels of the E3 ubiquitin ligase Parkin. Overexpression of *parkin* in the rat retina stimulated retinal mitophagy, which was also protective against glaucomatous retinal ganglion cell death (Dai et al., 2018). Our data show UCP2 to be a regulator of mitochondrial homeostasis, as increased expression prevents damage from oxidative stress, and reduced expression can initiate mitophagy to mitigate exogenous increases in oxidative stress.

Conclusions

Overall, we have arrived at a model of how *Ucp2* deletion may protect tissues from mitochondrial damage. *Ucp2* deletion increases membrane potential and consequently increases the generation of free radicals. Sub-lethal levels of free radicals are a signal for mitophagy (Frank et al., 2012), and so mitochondria that generate greater levels of free radicals select themselves for degradation through mitophagy. In bulk, this likely increases mitochondrial turnover and improves respiratory function for a tissue, leading to a reduction in free radicals that are generated by damaged mitochondria during glaucoma or possibly other pathogenic conditions.

Author Contributions Statement

DTH and CJB contributed conception and design of the study; DTH acquired, analyzed, interpreted the data, and wrote the first draft of the manuscript; DTH and CJB contributed to critical revision and final approval of the manuscript.

Conflict of Interest Statement

The authors declare no competing financial interests.

Acknowledgments

This work was supported by grants from the National Institutes of Health and the Macula Vision Research Foundation. The authors thank Angela Snyder for providing the mouse cartoon used in figures 1 and 3, as well as Drs Evgenya Popova, Gregory Yochum, and Ian Simpson for their critical review of and intellectual contributions to this manuscript.

Literature Cited

Adachi H, Tominaga H, Maruyama Y, Yoneda K, Maruyama K, Yoshii K, Kinoshita S, Nakano M, Tashiro K (2015) Stage-specific reference genes significant for quantitative PCR during mouse retinal development. Genes Cells 20:625-635.

Andrews ZB, Horvath B, Barnstable CJ, Elsworth J, Elseworth J, Yang L, Beal MF, Roth RH, Matthews RT, Horvath TL (2005) Uncoupling protein-2 is critical for nigral dopamine cell survival in a mouse model of Parkinson's disease. J Neurosci 25:184-191.

Arsenijevic D, Onuma H, Pecqueur C, Raimbault S, Manning BS, Miroux B, Couplan E, Alves-Guerra MC, Goubern M, Surwit R, Bouillaud F, Richard D, Collins S, Ricquier D (2000) Disruption of the uncoupling protein-2 gene in mice reveals a role in immunity and reactive oxygen species production. Nat Genet 26:435-439.

Barnstable CJ, Reddy R, Li H, Horvath TL (2016) Mitochondrial Uncoupling Protein 2 (UCP2) Regulates Retinal Ganglion Cell Number and Survival. J Mol Neurosci.

Boland MV, Quigley HA (2007) Risk factors and open-angle glaucoma: classification and application. J Glaucoma 16:406-418.

Bouillaud F, Couplan E, Pecqueur C, Ricquier D (2001) Homologues of the uncoupling protein from brown adipose tissue (UCP1): UCP2, UCP3, BMCP1 and UCP4. Biochim Biophys Acta 1504:107-119.

Carter-Dawson L, Shen F, Harwerth RS, Smith EL, Crawford ML, Chuang A (1998) Glutamine immunoreactivity in Müller cells of monkey eyes with experimental glaucoma. Exp Eye Res 66:537-545.

Cone FE, Steinhart MR, Oglesby EN, Kalesnykas G, Pease ME, Quigley HA (2012) The effects of anesthesia, mouse strain and age on intraocular pressure and an improved murine model of experimental glaucoma. Exp Eye Res 99:27-35.

Dai Y, Hu X, Sun X (2018) Overexpression of parkin protects retinal ganglion cells in experimental glaucoma. Cell Death Dis 9:88.

de Bilbao F, Arsenijevic D, Vallet P, Hjelle OP, Ottersen OP, Bouras C, Raffin Y, Abou K, Langhans W, Collins S, Plamondon J, Alves-Guerra MC, Haguenauer A, Garcia I, Richard D, Ricquier D, Giannakopoulos P (2004) Resistance to cerebral ischemic injury in UCP2 knockout mice: evidence for a role of UCP2 as a regulator of mitochondrial glutathione levels. J Neurochem 89:1283-1292.

Diano S, Matthews RT, Patrylo P, Yang L, Beal MF, Barnstable CJ, Horvath TL (2003) Uncoupling protein 2 prevents neuronal death including that occurring during seizures: a mechanism for preconditioning. Endocrinology 144:5014-5021.

Ding C, Wang P, Tian N (2011) Effect of general anesthetics on IOP in elevated IOP mouse model. Exp Eye Res 92:512-520.

Donadelli M, Dando I, Fiorini C, Palmieri M (2014) UCP2, a mitochondrial protein regulated at multiple levels. Cell Mol Life Sci 71:1171-1190.

Drew BG, Ribas V, Le JA, Henstridge DC, Phun J, Zhou Z, Soleymani T, Daraei P, Sitz D, Vergnes L, Wanagat J, Reue K, Febbraio MA, Hevener AL (2014) HSP72 is a mitochondrial stress sensor critical for Parkin action, oxidative metabolism, and insulin sensitivity in skeletal muscle. Diabetes 63:1488-1505.

Echtay KS, Winkler E, Frischmuth K, Klingenberg M (2001) Uncoupling proteins 2 and 3 are highly active H(+) transporters and highly nucleotide sensitive when activated by coenzyme Q (ubiquinone). Proc Natl Acad Sci U S A 98:1416-1421.

Ferreira SM, Lerner SF, Brunzini R, Reides CG, Evelson PA, Llesuy SF (2010) Time course changes of oxidative stress markers in a rat experimental glaucoma model. Invest Ophthalmol Vis Sci 51:4635-4640.

Fleury C, Neverova M, Collins S, Raimbault S, Champigny O, Levi-Meyrueis C, Bouillaud F, Seldin MF, Surwit RS, Ricquier D, Warden CH (1997) Uncoupling protein-2: a novel gene linked to obesity and hyperinsulinemia. Nat Genet 15:269-272.

Ganat YM, Silbereis J, Cave C, Ngu H, Anderson GM, Ohkubo Y, Ment LR, Vaccarino FM (2006) Early postnatal astroglial cells produce multilineage precursors and neural stem cells in vivo. J Neurosci 26:8609-8621.

Garcia-Medina JJ, Garcia-Medina M, Garrido-Fernandez P, Galvan-Espinosa J, Garcia-Maturana C, Zanon-Moreno V, Pinazo-Duran MD (2014) A two-year follow-up of oral antioxidant supplementation in primary open-angle glaucoma: an open-label, randomized, controlled trial. Acta Ophthalmol.

Haines BA, Mehta SL, Pratt SM, Warden CH, Li PA (2010) Deletion of mitochondrial uncoupling protein-2 increases ischemic brain damage after transient focal ischemia by altering gene expression patterns and enhancing inflammatory cytokines. J Cereb Blood Flow Metab 30:1825-1833.

Haslip M, Dostanic I, Huang Y, Zhang Y, Russell KS, Jurczak MJ, Mannam P, Giordano F, Erzurum SC, Lee PJ (2015) Endothelial uncoupling protein 2 regulates mitophagy and pulmonary hypertension during intermittent hypoxia. Arterioscler Thromb Vasc Biol 35:1166-1178.

Ju WK, Kim KY, Noh YH, Hoshijima M, Lukas TJ, Ellisman MH, Weinreb RN, Perkins GA (2015) Increased mitochondrial fission and volume density by blocking glutamate excitotoxicity protect glaucomatous optic nerve head astrocytes. Glia 63:736-753.

Kawasaki A, Otori Y, Barnstable CJ (2000) Müller cell protection of rat retinal ganglion cells from glutamate and nitric oxide neurotoxicity. Invest Ophthalmol Vis Sci 41:3444-3450.

Khawaja AP et al. (2016) Assessing the Association of Mitochondrial Genetic Variation With Primary Open-Angle Glaucoma Using Gene-Set Analyses. Invest Ophthalmol Vis Sci 57:5046-5052.

Kim I, Lemasters JJ (2011) Mitophagy selectively degrades individual damaged mitochondria after photoirradiation. Antioxid Redox Signal 14:1919-1928.

Kim I, Rodriguez-Enriquez S, Lemasters JJ (2007) Selective degradation of mitochondria by mitophagy. Arch Biochem Biophys 462:245-253.

Kimura A, Namekata K, Guo X, Noro T, Harada C, Harada T (2017) Targeting Oxidative Stress for Treatment of Glaucoma and Optic Neuritis. Oxid Med Cell Longev 2017:2817252.

Kong GY, Van Bergen NJ, Trounce IA, Crowston JG (2009) Mitochondrial dysfunction and glaucoma. J Glaucoma 18:93-100.

Korshunov SS, Skulachev VP, Starkov AA (1997) High protonic potential actuates a mechanism of production of reactive oxygen species in mitochondria. FEBS Lett 416:15-18.

Lapp DW, Zhang SS, Barnstable CJ (2014) Stat3 mediates LIF-induced protection of astrocytes against toxic ROS by upregulating the UPC2 mRNA pool. Glia 62:159-170.

Lee D, Shim MS, Kim KY, Noh YH, Kim H, Kim SY, Weinreb RN, Ju WK (2014) Coenzyme Q10 inhibits glutamate excitotoxicity and oxidative stress-mediated mitochondrial alteration in a mouse model of glaucoma. Invest Ophthalmol Vis Sci 55:993-1005.

Lee S, Van Bergen NJ, Kong GY, Chrysostomou V, Waugh HS, O'Neill EC, Crowston JG, Trounce IA (2011) Mitochondrial dysfunction in glaucoma and emerging bioenergetic therapies. Exp Eye Res 93:204-212.

Lemasters JJ (2005) Selective mitochondrial autophagy, or mitophagy, as a targeted defense against oxidative stress, mitochondrial dysfunction, and aging. Rejuvenation Res 8:3-5.

Malone PE, Hernandez MR (2007) 4-Hydroxynonenal, a product of oxidative stress, leads to an antioxidant response in optic nerve head astrocytes. Exp Eye Res 84:444-454.

Mattiasson G, Shamloo M, Gido G, Mathi K, Tomasevic G, Yi S, Warden CH, Castilho RF, Melcher T, Gonzalez-Zulueta M, Nikolich K, Wieloch T (2003) Uncoupling protein-2 prevents neuronal death and diminishes brain dysfunction after stroke and brain trauma. Nat Med 9:1062-1068.

Miwa S, St-Pierre J, Partridge L, Brand MD (2003) Superoxide and hydrogen peroxide production by Drosophila mitochondria. Free Radic Biol Med 35:938-948.

Moreno MC, Campanelli J, Sande P, Sánez DA, Keller Sarmiento MI, Rosenstein RE (2004) Retinal oxidative stress induced by high intraocular pressure. Free Radic Biol Med 37:803-812.

Mousa A, Kondkar AA, Al-Obeidan SA, Azad TA, Sultan T, Osman E, Abu-Amero KK (2015) Association of total antioxidants level with glaucoma type and severity. Saudi Med J 36:671-677.

Murphy JL, Ratnaike TE, Shang E, Falkous G, Blakely EL, Alston CL, Taivassalo T, Haller RG, Taylor RW, Turnbull DM (2012) Cytochrome c oxidase-intermediate fibres: importance in understanding the pathogenesis and treatment of mitochondrial myopathy. Neuromuscul Disord 22:690-698.

Nègre-Salvayre A, Hirtz C, Carrera G, Cazenave R, Troly M, Salvayre R, Pénicaud L, Casteilla L (1997) A role for uncoupling protein-2 as a regulator of mitochondrial hydrogen peroxide generation. FASEB J 11:809-815.

Pecqueur C, Alves-Guerra MC, Gelly C, Levi-Meyrueis C, Couplan E, Collins S, Ricquier D, Bouillaud F, Miroux B (2001) Uncoupling protein 2, in vivo distribution, induction upon oxidative stress, and evidence for translational regulation. J Biol Chem 276:8705-8712.

Pinzon-Guzman C, Zhang SS, Barnstable CJ (2011) Specific protein kinase C isoforms are required for rod photoreceptor differentiation. J Neurosci 31:18606-18617.

Quigley HA (2011) Glaucoma. Lancet 377:1367-1377.

Resnikoff S, Keys TU (2012) Future trends in global blindness. Indian J Ophthalmol 60:387-395.

Richard D, Clavel S, Huang Q, Sanchis D, Ricquier D (2001) Uncoupling protein 2 in the brain: distribution and function. Biochem Soc Trans 29:812-817.

Rodriguez AR, de Sevilla Müller LP, Brecha NC (2014) The RNA binding protein RBPMS is a selective marker of ganglion cells in the mammalian retina. J Comp Neurol 522:1411-1443.

Sappington RM, Carlson BJ, Crish SD, Calkins DJ (2010) The microbead occlusion model: a paradigm for induced ocular hypertension in rats and mice. Invest Ophthalmol Vis Sci 51:207-216.

Sarafian TA, Montes C, Imura T, Qi J, Coppola G, Geschwind DH, Sofroniew MV (2010) Disruption of astrocyte STAT3 signaling decreases mitochondrial function and increases oxidative stress in vitro. PLoS One 5:e9532.

Shen C, Chen L, Jiang L, Lai TY (2015) Neuroprotective effect of epigallocatechin-3-gallate in a mouse model of chronic glaucoma. Neurosci Lett.

Tanihara H, Hangai M, Sawaguchi S, Abe H, Kageyama M, Nakazawa F, Shirasawa E, Honda Y (1997) Up-regulation of glial fibrillary acidic protein in the retina of primate eyes with experimental glaucoma. Arch Ophthalmol 115:752-756.

Tham YC, Li X, Wong TY, Quigley HA, Aung T, Cheng CY (2014) Global prevalence of glaucoma and projections of glaucoma burden through 2040: a systematic review and meta-analysis. Ophthalmology 121:2081-2090.

Varela HJ, Hernandez MR (1997) Astrocyte responses in human optic nerve head with primary open-angle glaucoma. J Glaucoma 6:303-313.

Wei R, Stewart EA, Amoaku WM (2013) Suitability of endogenous reference genes for gene expression studies with human intraocular endothelial cells. BMC Res Notes 6:46.

Woldemussie E, Wijono M, Ruiz G (2004) Müller cell response to laser-induced increase in intraocular pressure in rats. Glia 47:109-119.

Wong-Riley M (1979) Changes in the visual system of monocularly sutured or enucleated cats demonstrable with cytochrome oxidase histochemistry. Brain Res 171:11-28.

Zhang CY, Baffy G, Perret P, Krauss S, Peroni O, Grujic D, Hagen T, Vidal-Puig AJ, Boss O, Kim YB, Zheng XX, Wheeler MB, Shulman GI, Chan CB, Lowell BB (2001) Uncoupling protein-2 negatively regulates insulin secretion and is a major link between obesity, beta cell dysfunction, and type 2 diabetes. Cell 105:745-755.

Zhang Y, Riesterer C, Ayrall AM, Sablitzky F, Littlewood TD, Reth M (1996) Inducible site-directed recombination in mouse embryonic stem cells. Nucleic Acids Res 24:543-548.

Figure Legends:

Figure 1. Expression of UCP2 in the retina and characteristics of the microbead model of glaucoma. (**A**) Representative immunohistochemical labeling of UCP2 in retinas from full-body UCP2-KO mice and wild-type mice, showing that UCP2 is distributed throughout the retina, but is expressed to a greater extent in the ganglion cell layer. (**B**) Schematic diagram representing the order of manipulations made to mice prior to and during the microbead model of glaucoma. Each arrow represents a different day. (**C**) Baseline (pre-bead injection) IOP compared between male and female C57BL6/J mice (left), showing no effect of gender on IOP. These data were pooled and

compared against baseline IOP in *Ucp2*$^{fl/fl}$ mice. In both cases there is no statistical difference in mean IOP (T-test). (**D**) We verified the location of microbeads following injection through the cornea, and found them packed between the cornea and iris, at the aqueous humor outflow pathway. (**E**) 30 days following IOP elevation, the difference in RGC density between PBS- and bead-injected eyes of Ucp2$^{fl/fl}$ mice was analyzed as a function of average IOP difference between those eyes, showing a positive correlation between IOP elevation and RGC loss.

Figure 2. Elevating intra-ocular pressure increases oxidative stress and decreases mitochondrial function. (A) 4-hydroxynonenal (green) and Hoechst 33258 (blue) labeling of retinal sections from PBS- and microbead-injected eyes, 30 days post-injection. (**B**) Quantification of immunoreactivity in different retinal layers reveals that HNE labeling is significantly greater within the inner retina of bead injected eyes, relative to contralateral PBS-injected control eyes (black bars=PBS-injected, red bars=bead-injected, n=5). (**C**) COX histochemistry of retinal sections from PBS- and microbead-injected eyes 3 days post-injection, showing that bead injection appears to decreases cytochrome C oxidase activity (DAB labeling) early in glaucoma (n=3). (**D**) mtDNA to nDNA ratio in bead-injected eyes relative to PBS-injected eyes early (3 days, n=3) and later (30 days, n=8) post-bead-injection. Over time, there appears to be a decrease in mitochondrial mass (mtDNA/nDNA). (**E**) Gene expression changes early in glaucoma show that (I) PBS-injection does not appear to significantly alter gene expression relative to untreated retinas, and (II) bead-injection increases the expression of several antioxidant and glaucoma-related genes, including Hmox1, Nfe2l2, and C1Qa (n=3). IS=Inner segments, ONL=outer nuclear layer, OPL=outer plexiform layer, INL=inner nuclear layer, IPL=inner plexiform layer, GCL=ganglion cell layer, RNFL=retinal nerve fiber layer, Outer=outer retina, Inner=inner retina. *=$p<0.05$, **=$p<0.01$.

Figure 3. *Cre*-mediated *Ucp2* excision increases ψ_m, the rate of oxidant generation, and mitochondrial oxygen consumption in primary astrocytes. (**A**) Schematic diagram of transgenic mouse genotypes for mice used in this study, the approximate primer locations for genotyping these animals, the region of DNA excised by Cre recombinase activity, tissues used from these mice, and the figures in which these tissues are used. (**B**) Example genotyping PCR of 4-hydroxytamoxifen pretreated astrocytes from *Ucp2*$^{fl/fl}$ (lanes 1-2) and *Ucp2*$^{fl/fl}$; *Gfap-creER*^{T2} (lanes 3-4) mice. The primers in this reaction only amplify when the >1000bp LoxP-flanked region of the Ucp2 gene is removed. (**C**) The JC-1 red/green fluorescence ratio in these primary astrocytes (n=8) in increased by UCP2 deletion (n=7) and decreased by 1μM FCCP (n=3), revealing that UCP2 normally functions to decrease ψ_m in these cells. (**D**) The rate of CM-H_2-DCFDA oxidation is also increased with *Ucp2* deletion (n=7) or with 4μM Antimycin A (n=5). (**E**) Seahorse XF96 measurement of cellular oxygen consumption demonstrating that *Ucp2* deletion increases the basal and maximal mitochondrial oxygen consumption of astrocytes, though not uncoupled respiration (n=3). *=$p<0.05$, ***=$p<0.005$.

Figure 4. *Ucp2* deletion in either glia or RGCs prevents RGC loss in glaucoma. (**A**) *Ucp2* expression in U*cp2*$^{fl/fl}$, *Ucp2*$^{fl/fl}$; *Gfap-creER*^{T2}, and *Ucp2*$^{fl/fl}$; *Thy1-creER*^{T2} retinas , showing a decrease in *Ucp2* expression in these transgenic mice (**B**) Whole-mount retinas labeled with the nuclear label Hoechst-33258 (blue), the retinal ganglion cell marker RBPMS (red), and the endogenous fluorescence of EGFP in *Gfap-creER*^{T2} mice (left) or YFP in *Thy1-creER*^{T2} mice (right). (**C**) IOP difference between microbead and PBS-injected *Ucp2*$^{fl/fl}$, *Ucp2*$^{fl/fl}$; *Gfap-creER*^{T2}, and *Ucp2*$^{fl/fl}$; *Thy1-creER*^{T2} eyes over time following a single microbead injection. (**D**) Example RBPMS-labeled RGCs in PBS- and Bead-injected eyes from *Ucp2*$^{fl/fl}$ (n=29), *Ucp2*$^{fl/fl}$; *Gfap-creER*^{T2} (n=10), and *Ucp2*$^{fl/fl}$; *Thy1-creER*^{T2} (n=13), with the differences in RGC density between PBS- and Bead-injected eyes is quantified in (**E**). A difference of “0” indicated no retinal ganglion cell death. **=p<0.01.

Figure 5. *Ucp2* deletion in glia or retinal ganglion cells decreases retinal oxidative stress, suppresses gliosis, and increases mtDNA/nDNA. (**A**) Representative 4-hydroxynonenal (green) and Hoechst33258 (blue)-labeled images and (**B**) quantification of 4-hydroxynonenal labeling in the inner retinas of bead-injected *Ucp2*$^{fl/fl}$ (n=8), *Ucp2*$^{fl/fl}$; *Gfap-creER*^{T2} (n=7), and *Ucp2*$^{fl/fl}$; *Thy1-creER*^{T2} eyes (n=8). These data show that the increase in 4-hydroxynonenal observed in glaucoma is prevented by UCP2-deletion in either RGCs or GFAP-expressing astrocytes and müller glia. (**C**) Retinal gliosis is increased in the bead-injected *Ucp2*$^{fl/fl}$ retina (n=23) but not in mice also expressing *Gfap-creER*^{T2} (n=13) or *Thy1-creER*^{T2} (n=7). (**D**) mtDNA/nDNA in retinal tissue from the above mice shows significantly greater levels of mtDNA/nDNA in *Ucp2*$^{fl/fl}$; *Thy1-creER*^{T2} (n=4) retinas than in *Ucp2*$^{fl/fl}$ (n=4) or *Ucp2*$^{fl/fl}$*; Gfap-creER*^{T2} retinas (n=8). *=p<0.05,**=p<0.01.

Figure 6. *Ucp2* deletion does not alter mitochondrial biogenesis and increases mitophagy. (**A**) mtDNA/nDNA in cultured primary cortical astrocytes sufficient and deficient in *Ucp2*, showing that UCP2 increases mtDNA/nDNA (n=3). (**B**) Expression of genes associated with mitochondrial biogenesis and function in cultured astrocytes, showing that *Ucp2* deletion does not increase biogenesis, but does decrease the expression of mitochondrial genes (n=4). Representative images (**C**) and quantification of colocalization (**D**) between LC3B (green) and Tomm20 (red) in *Ucp2*$^{fl/fl}$ (n=5) and *Ucp2*$^{fl/fl}$*; Gfap-creER*^{T2} astrocytes (n=3), showing a significant increase in colocalization with *Ucp2* deletion. Cell identity was confirmed using the astrocyte marker GFAP (white) and the DNA label Hoechst-3328 (blue). (**E**) Representative images showing the localization of IRF3 (red) in *Ucp2*$^{fl/fl}$ and *Ucp2*$^{fl/fl}$*; Gfap-creER*^{T2} primary cortical astrocytes marked by GFAP (green; n=3). *=p<0.05

Figure 7. Ucp2 deletion increases autophagy *in vivo* without altering mitochondrial biogenesis. (**A**) Expression of the mitochondrial biogenesis-related genes in retinas from *Ucp2*$^{fl/fl}$, *Ucp2*$^{fl/fl}$; *Gfap-creER*^{T2}, and *Ucp2*$^{fl/fl}$; *Thy1-creER*^{T2} mice. There was no significant change in expression of these genes between mouse lines, though there appears to be a trend towards a decrease in the expression of these factors in the retinas of *Ucp2*$^{fl/fl}$; *Gfap-creER*^{T2}, and *Ucp2*$^{fl/fl}$; *Thy1-creER*^{T2} mice (n=3). Quantification (**B)** and representative images (**C**) of Hoechst-33258 (blue) and LC3B

labeling (green) in retinas from *Ucp2*$^{fl/fl}$ (n=5), *Ucp2*$^{fl/fl}$; *Gfap-creER*^{T2} (n=3), and *Ucp2*$^{fl/fl}$; *Thy1-creER*^{T2} mice (n=3). **=p<0.01, ****=p<0.001.

Figure 8. The proposed model for Ucp2 deletion-mediated neuroprotection. Schematic diagram showing the interplay of oxidative stress, decreased mitochondrial function, decreased axonal transport, and altered glial cell activation, all of which are known to play pathophysiological roles in glaucoma and several other neurodegenerative conditions. These factors all contribute to each other and to retinal ganglion cell death. Our proposed mechanism to explain the protective effects of *Ucp2* deletion is by this alteration leading to a ROS-dependent increase in mitophagy, which disposes of damaged mitochondria, cutting short the cycle of degenerative phenomena.

Tables:

Table 1. Primers used in this study

Gene	Forward (5'→3')	Reverse (5'→3')	Citation*
Genotyping Primers, for use with genomic DNA			
Ucp2^{Flox}	ACCAGGGCTGTCTCCAAGCAGG	AGAGCTGTTCGAACACCAGGCCA	(Robson-Doucette et al., 2011)
Ucp2$^{\Delta}$	AGAGCTGTTCGAACACCAGGCCA	TAGAGGAGGGTGGTGTTCCAGCTC	(Robson-Doucette et al., 2011)
CreER^{T2}	GCAACGAGTGATGAGGTTCGCAAG	TCCGCCGCATAACCAGTGAAACAG	(Ganat et al., 2006)
RT-PCR primers, for use with cDNA			
Ucp2	GCTCAGAGCATGCAGGCATCG	CGTGCAATGGTCTTGTAGGCTTCG	
Sod2	TGGACAAACCTGAGCCCTAAG	CCCAAAGTCACGCTTGATAGC	(Masand et al., 2018)
Tfam	AAGGATGATTCGGCTCAGG	GGCTTTGAGACCTAACTGG	(Masand et al., 2018)
CytB	AGACAAAGCCACCTTGACCCGAT	ACGATTGCTAGGGCCGCGAT	(Tewari et al., 2012)
Nfe2l2	GTTGCCCACATTCCCAAAC	GCAAGCGACTCATGGTCATC	
Hmox1	GGGTGACAGAAGAGGCTAAGACC	GGGCAGTATCTTGCACCAGG	
PolgA	GCAGGATGGGCAGGAACA	GCATCCGGGAGTCCTGAA	(Masand et al., 2018)
C1Qa	GAGGGGAGCCAGGAGCTG	GGATTGCCTTTCACGCCC	
Pgc1α	AGCCGTGACCACTGACAACGAG	GCTGCATGGTTCTGAGTGCTAAG	(Masand et al., 2018)
Tbp	ACCTTATGCTCAGGGCTTGGCC	GTCCTGTGCCGTAAGGCATCATTG	(Perreten Lambert et al., 2014)

*Uncited primers are self-designed

Table 2. Antibodies used in this study

Protein	**Host**	**Dilution**	**Supplier**	**Cat#**
GFAP (N18)	Goat	1:200	Santa Cruz Biotechnology	sc-6171
GFAP (GA5)	Mouse	1:500	Cell Signaling Biotechnology	3670
GFAP	Rabbit	1:500	Dako	Z0334
HNEJ-2	Mouse	1:25	Abcam	ab48506
IRF3 (D6I4C)	Rabbit	1:200	Cell Signaling	11904
LC3B (D11)	Rabbit	1:200	Cell Signaling	3868
RBPMS	Rabbit	1:500	EMD Millipore	ABN1362
Tom20	Mouse	1:200	BD Biosciences	612278
Tom20	Rabbit	1:500	Abcam	ab78547

UCP2	Rabbit	1:100	MilliporeSigma	662047
AlexaFluor 488, Goat anti-rabbit	Goat	1:600	ThermoFisher	A11008
AlexaFluor 488, Goat anti-mouse	Goat	1:600	ThermoFisher	A11001
AlexaFluor 594, Goat anti-mouse	Goat	1:600	ThermoFisher	A11005
AlexaFluor 594, Goat anti-rabbit	Goat	1:600	ThermoFisher	A11012
AlexaFluor 647, Goat anti-mouse	Goat	1:600	ThermoFisher	A32728
DyLight 543, Donkey anti-Goat	Donkey	1:600	Vector Labs	DI-1549

Figure 1.

A

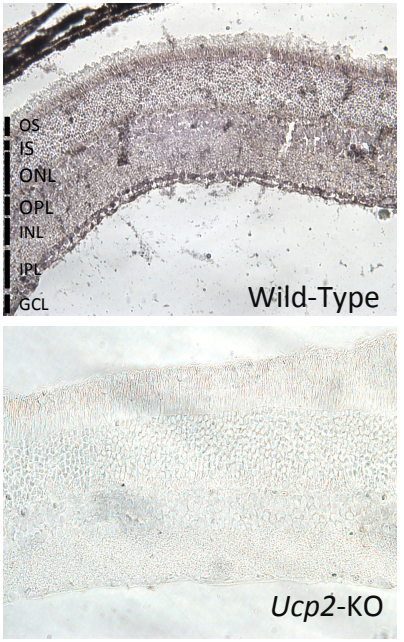

B

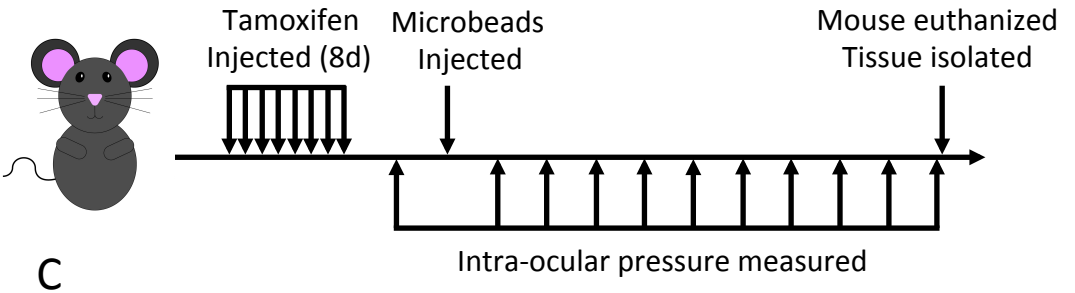

C

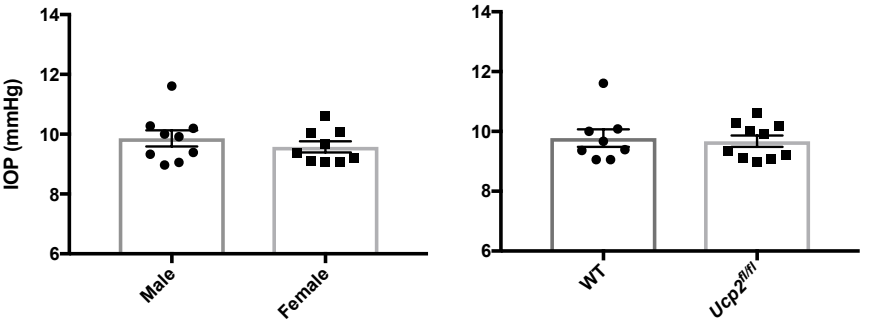

D

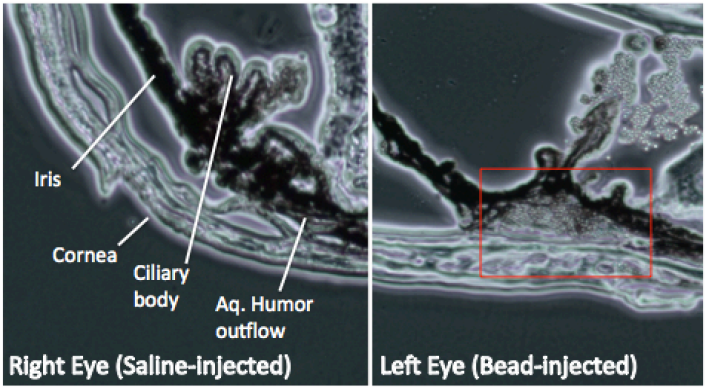

E

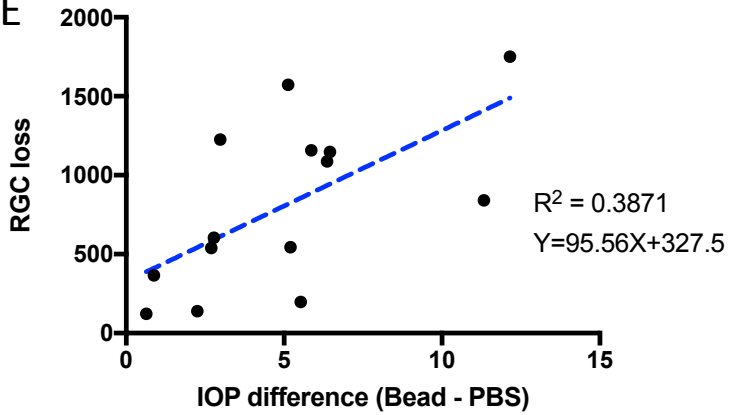

Figure 2.

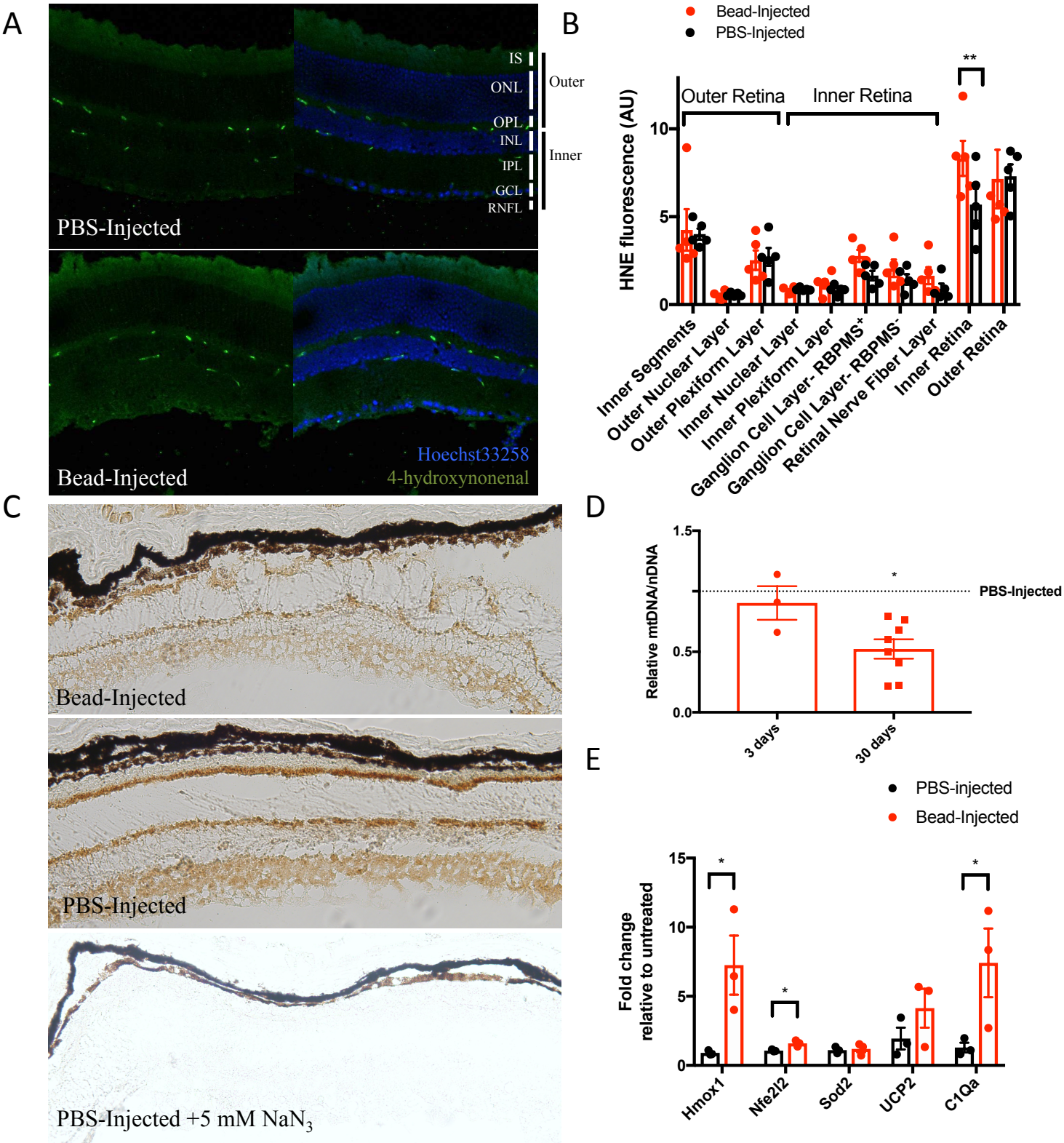
A
IS
ONL
OPL
INL
IPL
GCL
RNFL
Outer
Inner
PBS-Injected
Bead-Injected
Hoechst33258
4-hydroxynonenal
B
Bead-Injected
PBS-Injected
HNE fluorescence (AU)
Outer Retina
Inner Retina
**
Inner Segments
Outer Nuclear Layer
Outer Plexiform Layer
Inner Nuclear Layer
Inner Plexiform Layer
Ganglion Cell Layer- RBPMS+
Ganglion Cell Layer- RBPMS-
Retinal Nerve Fiber Layer
Inner Retina
Outer Retina
C
Bead-Injected
PBS-Injected
PBS-Injected +5 mM NaN3
D
Relative mtDNA/nDNA
PBS-Injected
3 days
30 days
E
PBS-injected
Bead-Injected
Fold change relative to untreated
Hmox1
Nfe2l2
Sod2
UCP2
C1Qa

Figure 3.

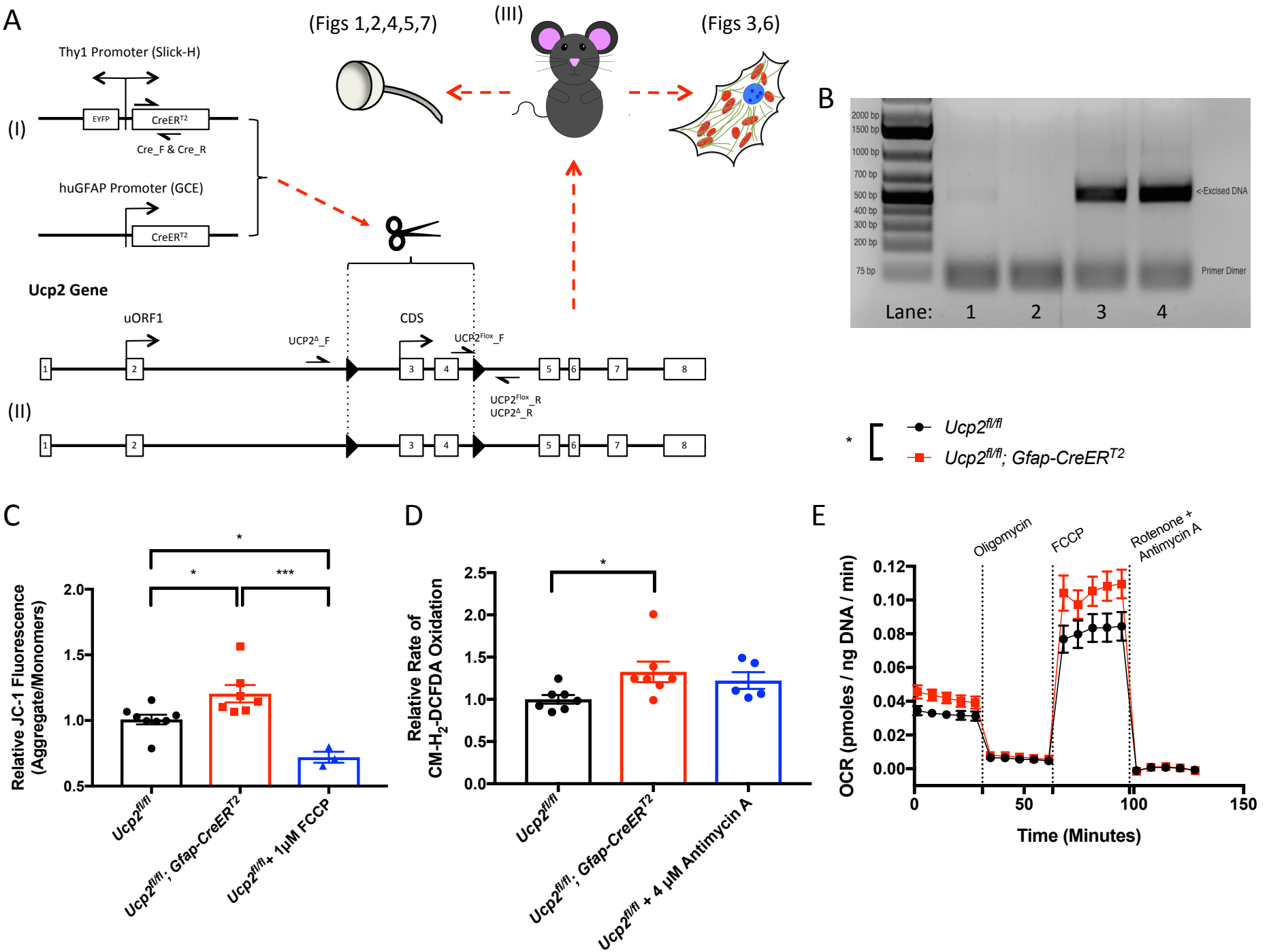
A
(Figs 1,2,4,5,7)
(III)
(Figs 3,6)
Thy1 Promoter (Slick-H)
(I)
EYFP
CreER^{T2}
Cre_F & Cre_R
huGFAP Promoter (GCE)
CreER^{T2}
Ucp2 Gene
uORF1
CDS
UCP2$^{\Delta}$_F
UCP2^{Flox}_F
UCP2^{Flox}_R
UCP2$^{\Delta}$_R
(II)
B
2000 bp
1500 bp
1000 bp
700 bp
500 bp
400 bp
300 bp
200 bp
75 bp
<-Excised DNA
Primer Dimer
Lane: 1 2 3 4
*
Ucp2$^{fl/fl}$
Ucp2$^{fl/fl}$; Gfap-CreER^{T2}
C
Relative JC-1 Fluorescence (Aggregate/Monomers)
Ucp2$^{fl/fl}$
Ucp2$^{fl/fl}$; Gfap-CreER^{T2}
Ucp2$^{fl/fl}$+ 1μM FCCP
D
Relative Rate of CM-H$_2$-DCFDA Oxidation
Ucp2$^{fl/fl}$
Ucp2$^{fl/fl}$; Gfap-CreER^{T2}
Ucp2$^{fl/fl}$ + 4 μM Antimycin A
E
Oligomycin
FCCP
Rotenone + Antimycin A
OCR (pmoles / ng DNA / min)
Time (Minutes)

Figure 4.

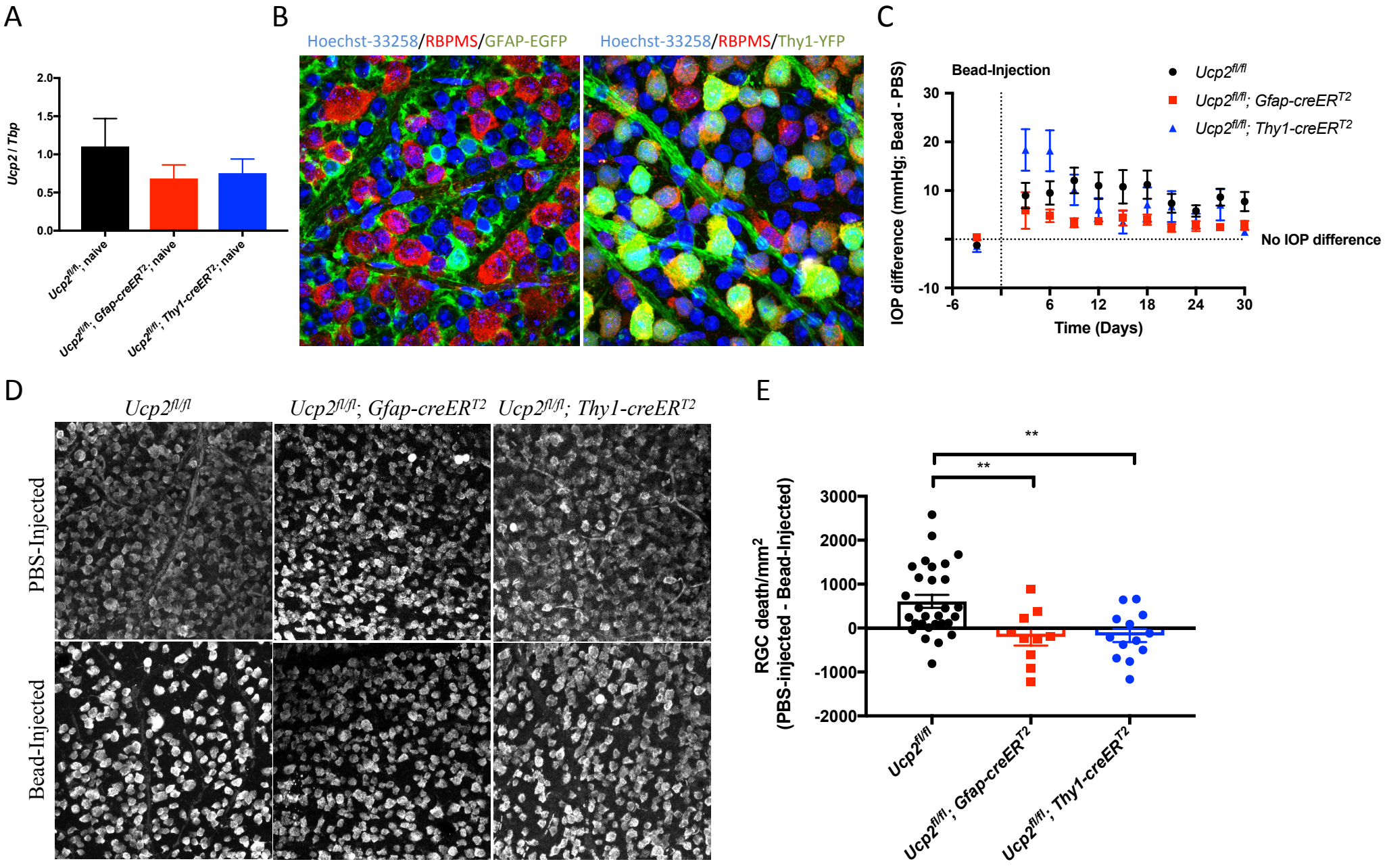
A
Ucp2 / Tbp
2.0
1.5
1.0
0.5
0.0
Ucp2fl/fl, naive
Ucp2fl/fl; Gfap-creERT2; naive
Ucp2fl/fl; Thy1-creERT2; naive
B
Hoechst-33258/RBPMS/GFAP-EGFP
Hoechst-33258/RBPMS/Thy1-YFP
C
Bead-Injection
Ucp2fl/fl
Ucp2fl/fl; Gfap-creERT2
Ucp2fl/fl; Thy1-creERT2
IOP difference (mmHg; Bead - PBS)
30
20
10
-10
No IOP difference
-6
6
12
18
24
30
Time (Days)
D
Ucp2fl/fl
Ucp2fl/fl; Gfap-creERT2
Ucp2fl/fl; Thy1-creERT2
PBS-Injected
Bead-Injected
E
**
**
RGC death/mm2
(PBS-injected - Bead-Injected)
3000
2000
1000
0
-1000
-2000
Ucp2fl/fl
Ucp2fl/fl; Gfap-creERT2
Ucp2fl/fl; Thy1-creERT2

Figure 5.

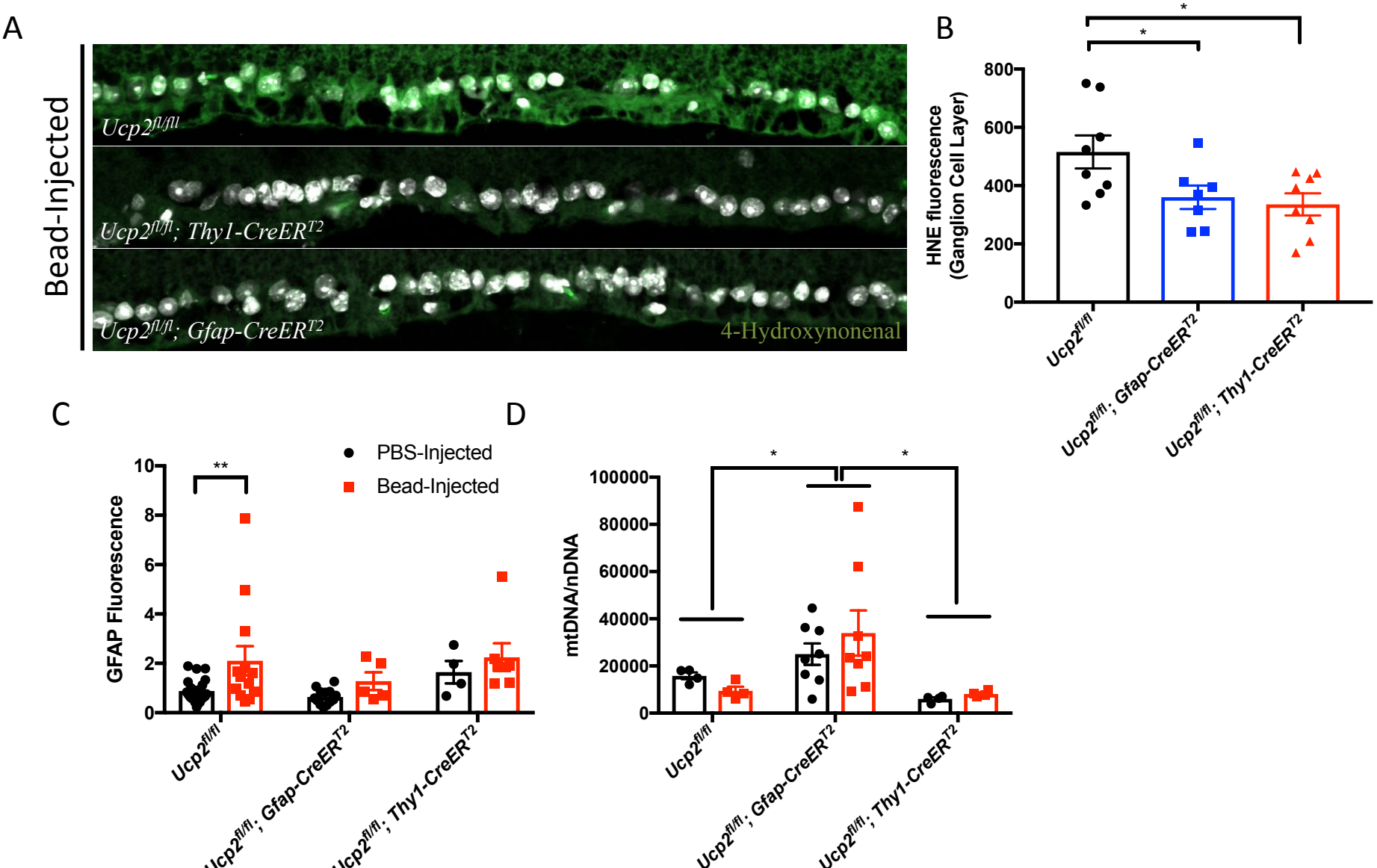
A
Bead-Injected
Ucp2fl/fl
Ucp2fl/fl; Thy1-CreERT2
Ucp2fl/fl; Gfap-CreERT2
4-Hydroxynonenal
B
HNE fluorescence (Ganglion Cell Layer)
800
600
400
200
0
*
*
Ucp2fl/fl
Ucp2fl/fl; Gfap-CreERT2
Ucp2fl/fl; Thy1-CreERT2
C
PBS-Injected
Bead-Injected
GFAP Fluorescence
10
8
6
4
2
0
**
Ucp2fl/fl
Ucp2fl/fl; Gfap-CreERT2
Ucp2fl/fl; Thy1-CreERT2
D
mtDNA/nDNA
100000
80000
60000
40000
20000
0
*
*
Ucp2fl/fl
Ucp2fl/fl; Gfap-CreERT2
Ucp2fl/fl; Thy1-CreERT2

Figure 6.

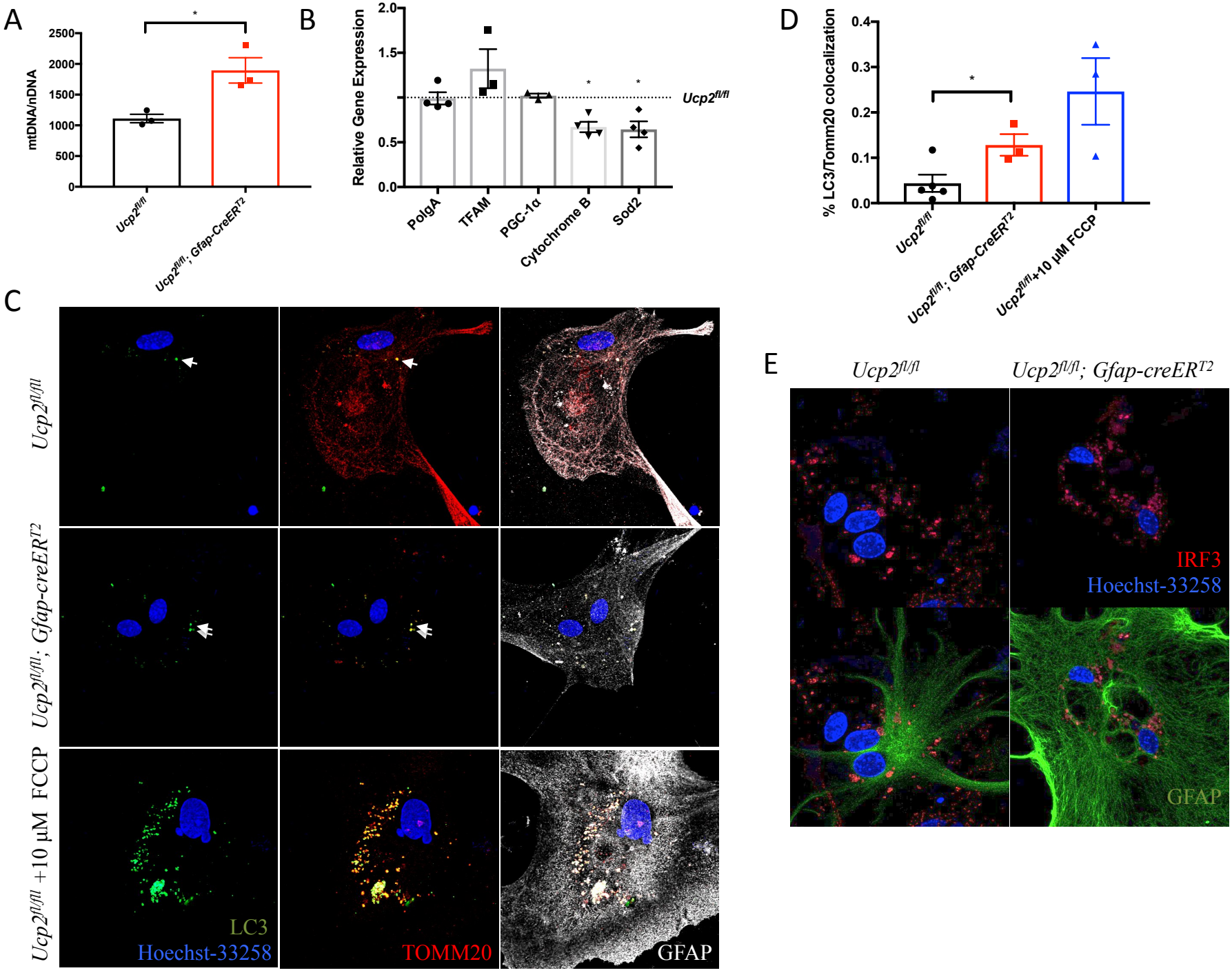
A
mtDNA/nDNA
2500
2000
1500
1000
500
0
*
Ucp2fl/fl
Ucp2fl/fl; Gfap-CreERT2
B
Relative Gene Expression
2.0
1.5
0.5
0.0
Ucp2fl/fl
PolgA
TFAM
PGC-1α
Cytochrome B
Sod2
D
% LC3/Tomm20 colocalization
0.4
0.3
0.2
0.1
0.0
Ucp2fl/fl
Ucp2fl/fl; Gfap-CreERT2
Ucp2fl/fl+10 μM FCCP
C
Ucp2fl/fl
Ucp2fl/fl; Gfap-creERT2
Ucp2fl/fl +10 μM FCCP
LC3
Hoechst-33258
TOMM20
GFAP
E
Ucp2fl/fl
Ucp2fl/fl; Gfap-creERT2
IRF3
Hoechst-33258
GFAP

Figure 7.

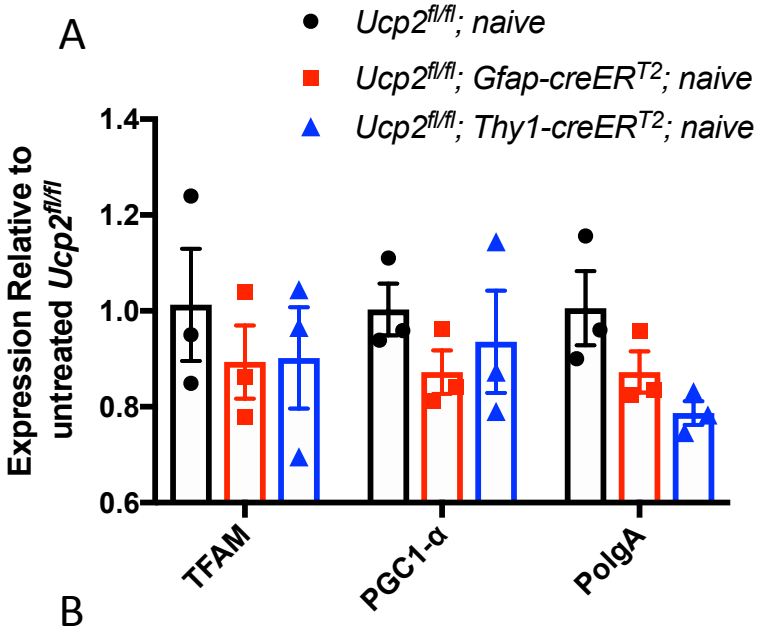
A
Ucp2fl/fl; naive
Ucp2fl/fl; Gfap-creERT2; naive
Ucp2fl/fl; Thy1-creERT2; naive
Expression Relative to untreated Ucp2fl/fl
1.4
1.2
1.0
0.8
0.6
TFAM
PGC1-α
PolgA

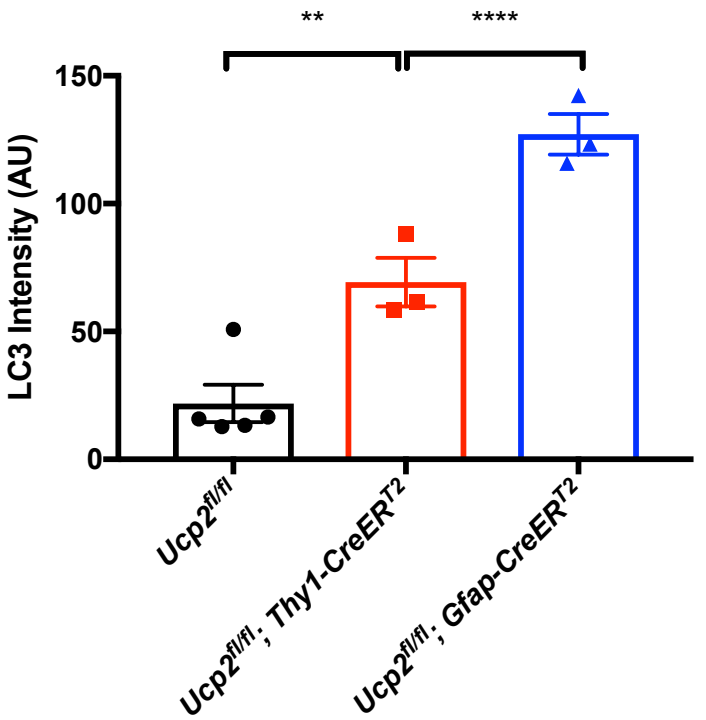
B
**
****
LC3 Intensity (AU)
150
100
50
0
Ucp2fl/fl
Ucp2fl/fl; Thy1-CreERT2
Ucp2fl/fl; Gfap-CreERT2

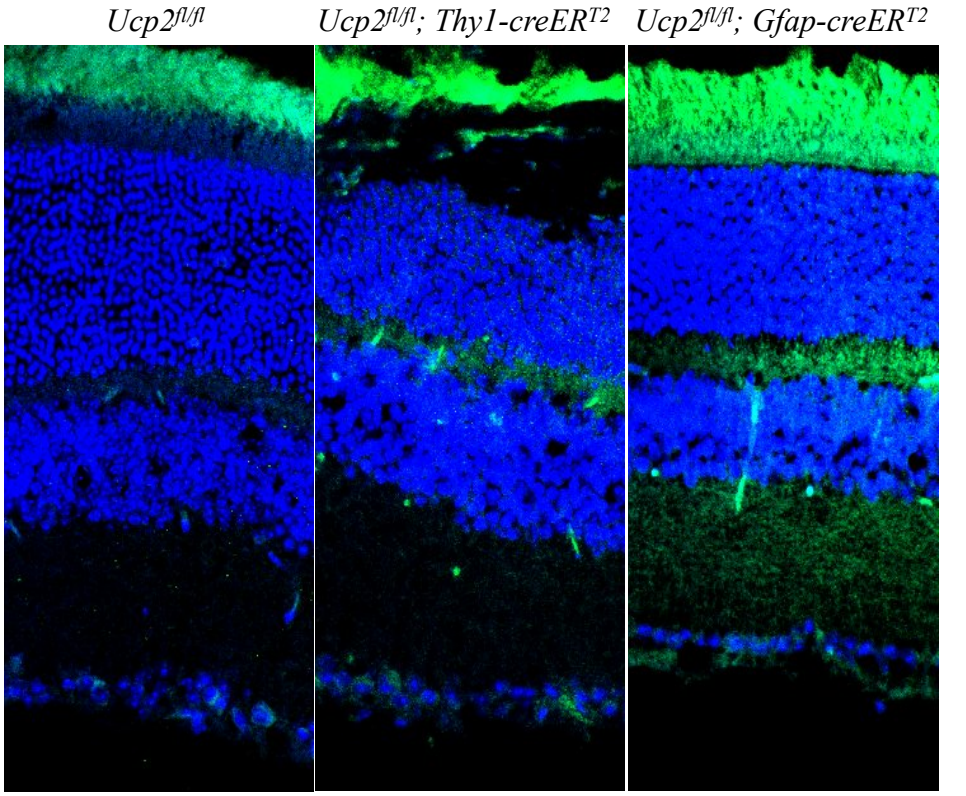
C
Ucp2fl/fl
Ucp2fl/fl; Thy1-creERT2
Ucp2fl/fl; Gfap-creERT2

Figure 8.

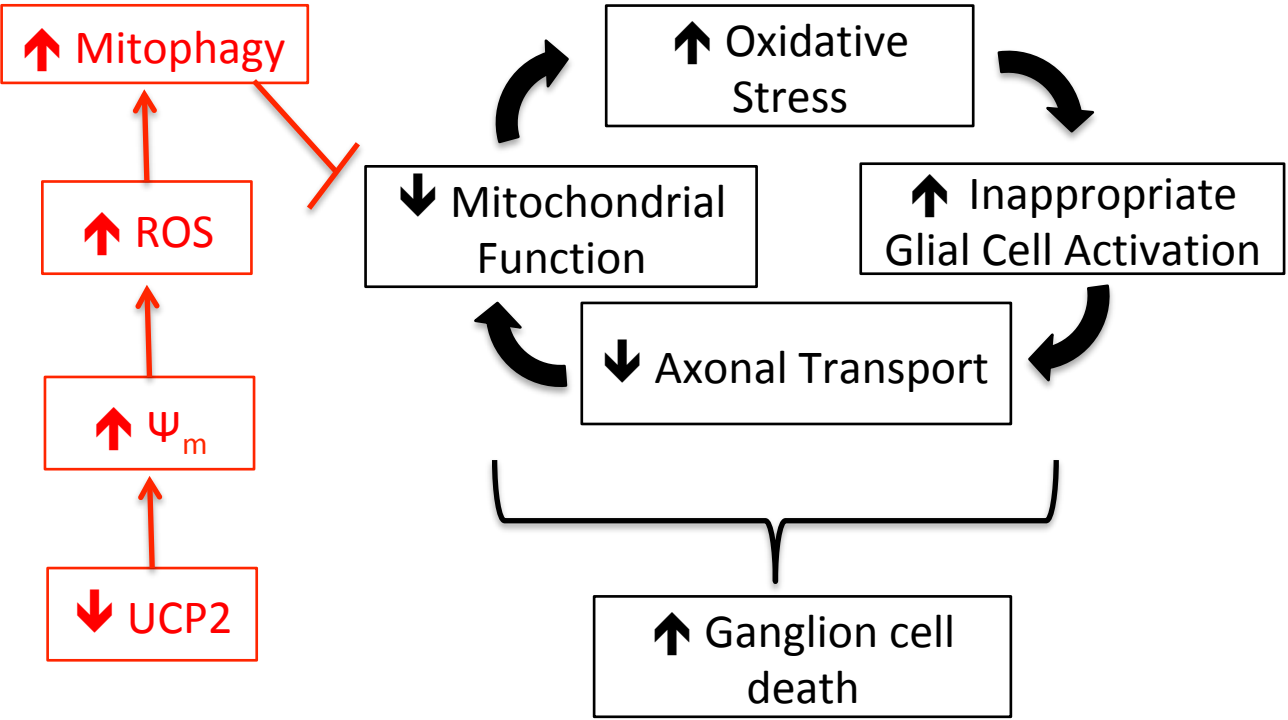
↑ Mitophagy
↑ ROS
↑ Ψm
↓ UCP2
↑ Oxidative Stress
↓ Mitochondrial Function
↑ Inappropriate Glial Cell Activation
↓ Axonal Transport
↑ Ganglion cell death